Label-free Quantification of Microscopic Alignment in Engineered Tissue Scaffolds by Polarized Raman Spectroscopy

Hui Zhou[+] - *Mechanical and Aerospace Engineering, University of Florida, Gainesville, Florida 32611, United States*

Janny Piñeiro Llanes - *J. Crayton Pruitt Family Department of Biomedical Engineering, University of Florida, Gainesville, Florida 32611, United States*

Maedeh Lotfi - *Mechanical and Aerospace Engineering, University of Florida, Gainesville, Florida 32611, United States*

Malisa Sarntinoranont - *Mechanical and Aerospace Engineering, University of Florida, Gainesville, Florida 32611, United States*

Chelsey S. Simmons - *Mechanical and Aerospace Engineering·, University of Florida, Gainesville, Florida 32611, United States*

Ghatu Subhash* - *Mechanical and Aerospace Engineering, University of Florida, Gainesville, Florida 32611, United States*

[+]Current Address: Collage of Polymer Science and Engineering, State Key Laboratory of Polymer Materials and Engineering, Sichuan University, Chengdu, 610065

*Corresponding Author, Email: subhash@ufl.edu

ABSTRACT

Monitoring of extracellular matrix (ECM) microstructure is essential in studying structure-associated cellular processes, improving cellular function, and for ensuring sufficient mechanical integrity in engineered tissues. This paper describes a novel method to study microscale alignment of matrix in engineered tissue scaffolds (ETS) that were usually composed of a variety of biomacromolecules derived by cells. First, a trained loading function was derived from Raman spectra of highly aligned native tissue via principal component analysis (PCA), where prominent changes associated with specific Raman bands (e.g., 1444, 1465, 1605, 1627-1660 and 1665-

1689 cm^{-1}) were detected with respect to the polarization angle. These changes were mainly caused by the aligned matrix of many compounds within the tissue relative to the laser polarization, including proteins, lipids, and carbohydrates. Hence this trained function was applied to quantify the alignment within ETS of various matrix components derived by cells. A simple metric called Amplitude Alignment Metric (AAM) was derived to correlate the orientation dependence of polarized Raman spectra of ETS to the degree of matrix alignment. It was found that the AAM was significantly higher in anisotropic ETS than isotropic ones. The PRS method revealed a lower *p*-value for distinguishing the alignment between the two types of ETS as compared to the microscopic method for detecting fluorescent-labeled protein matrices at similar microscopic scale. These results indicate that the anisotropy of complex matrix in engineered tissue can be assessed at microscopic scale using a PRS-based simple metric which is superior to traditional microscopic method. This PRS-based method can serve as a complementary tool for the design and assessment of engineered tissues that mimic the native matrix organizational microstructures.

KEYWORDS: *polarized Raman spectroscopy, principal component analysis, extracellular matrix, matrix alignment, engineered tissue scaffolds, anisotropy*

Introduction

Tissue-engineered systems provide convenient *in vitro* platforms to study cellular and molecular biology, in addition to their idealized role as implantable tissue replacements. One rich avenue of investigation is structure–function relationships in tissues,[1–4] since tissue architecture can influence biological processes ranging from cell proliferation[5] and migration[6,7] to cell fate[8,9] and

cancer progression.[10,11] To study the effect of extracellular matrix (ECM) organization on cell behaviors, it is critical to monitor this organization. In reality, ECM derived by cells in tissue engineering contains a variety of biomacromolecules, which can be hard to label one by one to monitor the alignment of each component. Typically, histological and immunohistochemical assays are used to evaluate the alignment of engineered tissue scaffolds (ETS); however, these methods usually require endpoint labeling for specific protein and extensive optimization. Besides, characterization of alignment should be done non-destructively and in a label-free manner with minimal changes of the structure and compositions within the engineered tissue. More recently, several label-free techniques have been developed to characterize the alignment in engineered tissue constructs, including second harmonic generation (SHG) [12] and polarized light microscopy.[13] However, these techniques are often limited to tissues rich in fibrillar collagen. For example, SHG is unable to detect collagen with small fiber diameters, non-fibrillar collagen, and other proteins due their negligible or very weak SHG signals.[12] Polarized light microscopy is also limited to collagen orientation. Polarized Raman spectroscopy (PRS) can overcome the above limitation because it can detect alignment at the molecular level as it is based on vibrational light-scattering technique in which the intensity of the signal relies on the orientation of vibrating molecules relative to the laser polarization direction. [14] Hence, PRS can extract structural information not only about collagen but all other biomacromolecules, such as multiple proteins and other cell components.[15] Since PRS can be performed in aqueous environments, it holds a distinct advantage over polarized Fourier-transform infrared spectroscopy in probing highly hydrated tissue samples.[16] In our own[17] and other studies,[18–20] PRS has been used to characterize the organization of matrix in native tissue. However, it seldomly has been applied to organizational matrix characterization of engineered tissue.

Bergholt et al., has applied PRS to characterize collagen orientation in native articular cartilage but was unable to measure organization of collagen in engineered cartilage due to a dominant water signal.[21] In this study, we report the first application of PRS to quantify the alignment in engineered scaffolds, including not only the collagen but all the ECM matrices and cell components in the scaffolds.

Raman spectroscopy detects the intensity of scattered light after the incident laser light interacts with molecular vibration modes within molecules comprising the sample. The position (wavenumber) of Raman bands in the spectra can be assigned to the molecular vibrations of chemical bonds within the molecules. PRS relies on intensity variations which can be further related to alignment in samples. For anisotropic samples (directionally oriented), the orientation of chemical bonds can be detected by rotating the sample with respect to the light polarization direction until the Raman spectral intensities from those bonds are maximized. On the contrary, when the bonds are oriented perpendicular to polarization direction, the intensities become minimal. For totally isotropic samples (randomly oriented), the chemical bonds are uniformly aligned in all directions and hence, the intensities of these bonds become fairly unchanged as the percentage of bonds oriented in each polarization direction is almost the same. Hence the variance of Raman intensities among different polarized angles is positively correlated to the degree of sample alignment. Based on this principle, two types of alignment in engineered scaffolds were generated to test if this PRS method can distinguish different alignment in the scaffolds of complex matrix compositions: (i) anisotropic engineered tissue scaffolds (aETS) and (ii) isotropic engineered tissue scaffolds (iETS). For aETS, aligned matrix was produced by culturing cardiac fibroblasts on micropatterned PDMS, where microchannel structures

encouraged cell reorganization and led to matrix assemblies with uniaxial aligned architecture. For iETS as control, the scaffolds were formed by cells plated on flat PDMS, where the cells deposited on randomly oriented matrices. The ECM deposited by cardiac fibroblasts is usually comprised of complex fibrillar proteins, non-fibrillar protein, other matrix biomacromolecules, and growth factors which can closely mimic the composition of native ECM microenvironments.[22,23] However, such matrix of various components can lead to broad and overlapping Raman bands, which is hard to accurately deconvolute into a single band for typical univariate analyses.[24] As univariate approaches are based on intensity (or area under the curve) of a single band assigned to a single matrix component, it is not suitable to apply to such complex matrix containing different components. To accommodate the complex composition of ETS containing varying matrix components, PRS coupled with multivariate principal component analysis (PCA) was used to decompose its Raman spectrum into a single variable. This variable called PC1 (principal component 1) captures the variation of original spectra among different polarized angles that can be quantified and related to the degree of matrix alignment. To accomplish this, a sine fitting function was used to derive a metric-called Amplitude Alignment Metric (AAM) defining the extent of variation of PC1. Our ultimate goal is to use a single metric to quantify the degree of alignment in ETS based on their polarized Raman spectra and trained PCA model. The ETS described herein is only a representative example of engineered tissue with complex compositions and the characterization method described can be applied to a broad range of engineered tissue constructs of different compositions and organization. To compare this PRS method to other traditional microscope method, a feature-based image analysis of immunofluorescent-labeled proteins was also investigated on ETS samples. Overall, the method used here for characterizing alignment in engineered scaffolds is mainly divided into

four parts: (1) ETS preparation, (2) PRS acquisition, (3) preprocessing and PCA analysis, (4) feature-based image analysis and (5) statistical analysis. In the following section, we will briefly discuss these steps.

Materials and Methods

1. Engineered tissue prepared for PRS

To replicate the aligned architecture of native muscle, micro-patterns (Fig. 1A) were fabricated on surfaces of PDMS which guides cells to generate anisotropic ECM. First, one needs to design the layout of the microchannel using a vector-based graphics software Illustrator 2021 (Adobe, San Joe, CA, USA). After printing the layout, a 10 cm mother silicon wafer was created using SU-8-2035 photoresin (Micro Chem, Y1110700500L1GL) by masking, lithographing, and dry etching as in previously described standard soft lithography techniques.[25] This results in 20μm × 20μm × 20μm channels on the final master mold (Fig. 1B). The dimension of 20μm (approximate the width of two cells) was chosen to allow the alignment of cells along the microchannel structure and cell-cell interactions as well. The master mold surface was treated with trichloro perfluorooctyl silane (Sigma Aldrich, 440191) to prevent further adhesion of PDMS and aid in the release of PDMS from the surface of the master mold. This master mold was then used to fabricate PDMS molds. Briefly, PDMS (Sylgard 184) with a curing agent at a weight ratio of 10:1 was poured into the master mold and cured for 48h at room temperature under vacuum. Then, the PDMS was detached from the master mold and punched into a 10cm diameter disk while an isotropic disk was cut from unpatterned parts of the same casted PDMS as control. The bright field images of the patterned and flat PDMS disks were shown in Fig. 1C and Fig. 1D, respectively.

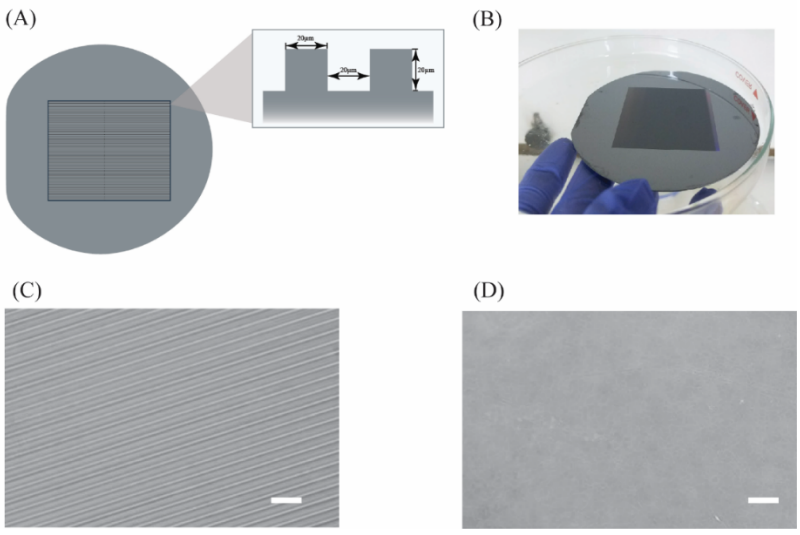

Figure 1. Fabrication and transferring micropatterns on PDMS. (A). Design of micropattern, (B) silicon master wafer with 20μm×20μm ×20μm channels and (C) bright field images of patterned PDMS with microtopographic lines and (D). flat PDMS mold. Scale bar = 50 μm.

For preparation of cell seeding, PDMS and coverslips of 12-cm diameter were treated to increase hydrophilicity via a UV curing system (IntelliRay 400; Uvitron International, West Springfield, MA, USA) for 60s at 115wW/cm^2. To aid in handling, PDMS stamps were mounted on 12-cm diameter coverslips after plasma treatment. They were immediately placed in DI water and sterilized for 20 min at 121˚C. The sterilized PDMS surface on coverslips was coated with 0.1% gelatin to enhance cell attachment before cell seeding. Here cardiac fibroblasts were used to deposit cardiac muscle ECM. The preparation of human pluripotent stem-cell derived cardiac fibroblasts (hPSC-CFs) was described in supporting information (see methods in Appendix 1).

To prepare aETS and iETS, a sacrificial layer of hPSC-CFs at a density of ~3×10^4 cells/cm^2 was plated on patterned PDMS and on flat PDMS, respectively. The cells on PDMS were cultured in cardiac fibroblast medium (Cell Application Inc., 316-500) for 24h in an incubator at 37˚C and

5% CO_2. After 24h, the medium was replaced by a fresh cardiac fibroblast matrix medium. For the first 5 days, media were changed every two days. After day 5, half-media changes were done every day. The samples were checked every day during the culture to ensure no detachment of cells (Fig. S1A-S1D). After 14 days without passaging cells, both aETS and iETS were fixed in 4% paraformaldehyde and then transferred to a glass slide for further characterization (Fig. 2A-2D).

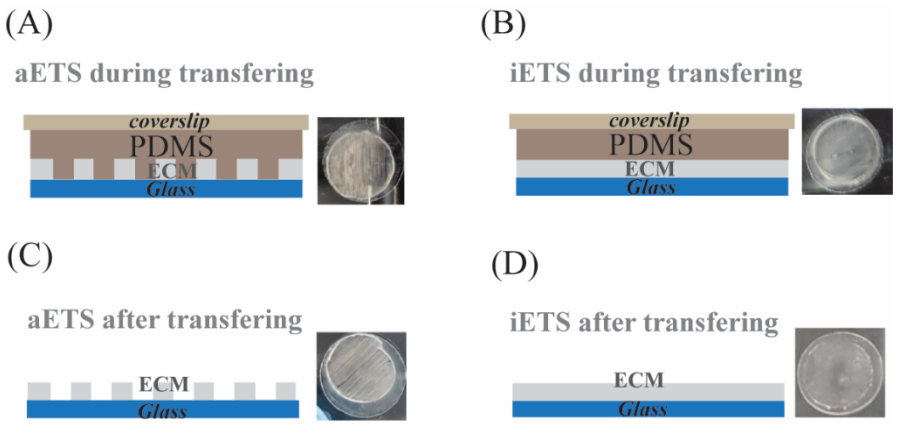

Figure 2. The schematic illustrating the process of transferring ETS on glass slide. (A) aETS and (B) iETS with the sample sides facing down on clean glass slides during the transferring. And then (C) aETS and (D) iETS were transferred to glass slides. The insets were the physical photos of ETS samples correspondingly.

2. PRS data acquisition

PRS is of particular utility for analyzing molecular alignment as it relies on polarized laser to incite Raman scattering, and the relative orientation of vibrations of e molecules to the laser polarization direction can influence the Raman signal intensity. To determine alignment of engineered tissues, spectra of different orientations were collected to understand the relation of

intensity variations to tissue alignment. Hence, PRS scans were performed at different polarized angles by rotating the ETS sample while keeping the polarizer at a set angle, as shown in Fig. 3. The polarized angle was defined as the angle θ between laser polarization direction (which is fixed horizontally) and the sample alignment axis (along the macroscopic dimension of the sample). For each region of interest (ROI), a total rotation of 180˚ can capture anisotropy in the sample regardless of whether the sample orientation is known due to the natural periodicity of protein fiber distributions.

The use of a PRS coupled with an optical microscope allows the user to obtain PRS measurements at precise locations inside the microchannels in ETS. Hence, a white light video was launched before or after spectral acquisition, which help define each ROI (11 data points) on the sample surface and ensure the scanning for the same ROI while rotating the sample by 30˚ each time between 0˚ and 180˚ (Fig. S2). For each polarized angle, 2 ROIs that are near each other are measured and the measurement for each ROI was performed at the same parameters (see Table S1). When each measurement is finished, we subtracted the baseline for removing fluorescent backgrounds by using "Intelligent fitting" applied with a polynomial order of 11 in Reishaw Raman WIRE® 4.4 software shown in Fig. S3. To subtract the contribution of PBS buffer solution as well, spectra of PBS background were measured 5 times for each polarized angle by moving the laser beside the sample region without changing the focus. The measurement parameters are kept the same as those in mapping measurement, except for selecting "5" acquisitions. The PBS spectra was saved for further subtraction which was shown in the next section of preprocessing.

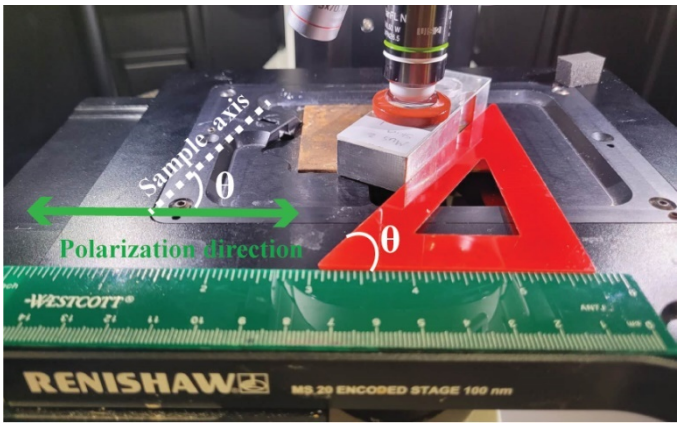

Figure 3. An example of PRS measurement at a polarized angle θ of 60˚. The glass slide was glued on an aluminium holder and the rubber gasket was used to immerse the ETS samples in PBS. The polarization angle was incremented by 30˚ while rotating the holder using the 30/60degree set square.

3. Data preprocessing and PCA analysis

The spectra obtained were first preprocessed using the following procedure: (i) subtraction of PBS background, (ii) smoothing, and (iii) standard normal variate (SNV) normalization. The purpose of preprocessing raw data is to help decrease variation in the Raman spectra that may be related to varying experimental conditions (e.g., inconsistent sample thickness, unwanted noises, etc.). The schematic of preprocessing and PCA analysis on Raman spectra of ETS are shown in Fig.4. First, each Raman spectrum in the range of 1400-1,800 cm^{-1} containing intensity values of 403 wavenumbers, was subtracted from the spectrum of PBS background averaged from five locations as mentioned in the previous section. To increase the signal-to-noise ratio embedded in a given dataset, these spectra, after subtracting PBS background, were further smoothed by Savitzky-Golay (SG) filter. Here, the SG filter is a successive local polynomial fitting to sub-sets of adjacent data points by the method of linear least squares. The intensities in each Raman

spectrum were replaced by the dot product of deconvolution coefficients from polynomial fitting and the neighbouring intensity values arriving at regularly spaced intervals. Here SG filter was chosen with a polynomial order of 3 and window size of 11 using Sgolayfilt function in Matlab. Lastly, the smoothed spectra were processed with standard normal variate (SNV) normalization for minimizing unwanted variations. Specifically, if the Raman wavenumber (or Raman band, unit: cm^{-1}) is stored in a vector, $s = (s_1, s_2, s_3, \ldots, s_N)$ for a single spectrum after smoothing, where the subscript *i* refers to a specific wavenumber in the range of 1400-1800 cm^{-1}. Hence the vector normalization is performed as:

$$\text{Mean} = (s_{1+}s_{2+}s_{3+\cdots+}s_N)/\text{N} \quad (1)$$

$$\text{SD} = \sqrt{(s_1 - mean)^2 + (s_2 - mean)^2 + (s_3 - mean)^2 \pm \cdots (s_N - mean)^2/(N-1)} \quad (2)$$

$$sn_i = (s_i - mean)/SD;\ i = 1,2,3, \ldots N \quad (3)$$

Each element s_i (sn_i) of the vector represents the Raman intensity of a given wavenumber before the normalization (after normalization). Finally, each spectrum was finally transformed into a single PC1 Score value. All these preprocessing steps were implemented in MATLAB® R2020a (The MathWorks, Inc., Natick, MA, USA) shown in Appendix S2. Each ROI contains 11 spectra from 11 different locations acquired in ETS. Hence the MATLAB code was run each time for a dataset of 154 sample spectra for 2 ROIs (22 spectra × 7 polarized angles). Here, an example of Raman spectra after being preprocessed in each step is shown in Fig. 5. The raw data of these Raman spectra can be found in the supporting information.

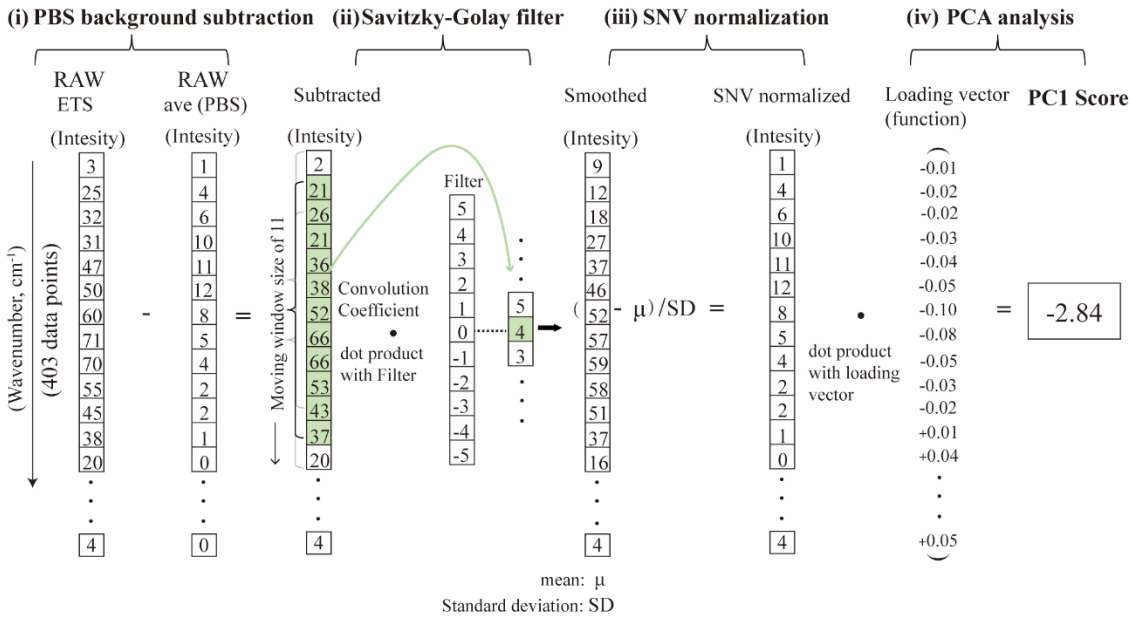

Figure 4. A schematic diagram of preprocessing steps and PCA analysis. Each spectrum contains intensity values of 403 wavenumbers in the range of 400-1800 cm^{-1}. In the PBS background subtraction(i), the intensities in each raw spectrum were subtracted by an averaged PBS spectrum. For Savitzky-Golay filter(ii), the intensity values of 11 neighbors were used to fit a polynomial to derive convolution coefficients which were multiplied (dot product) with these intensity values arriving at regularly spaced intervals. The centered original data in this 11-point moving window was replaced by the dot product so that it was locally averaged with surrounding intensities. For SNV normalization(iii), each intensity of the spectrum was subtracted by the mean of the spectrum and then divided by the standard deviation of the spectrum. Lastly, each intensity of the spectrum was multiplied (dot product) by a master loading function (vector) and the scalar product is the obtained single PC1 Score for the spectrum. In the supporting information, the raw ASCII data of ETS spectra and PBS spectra can be found.

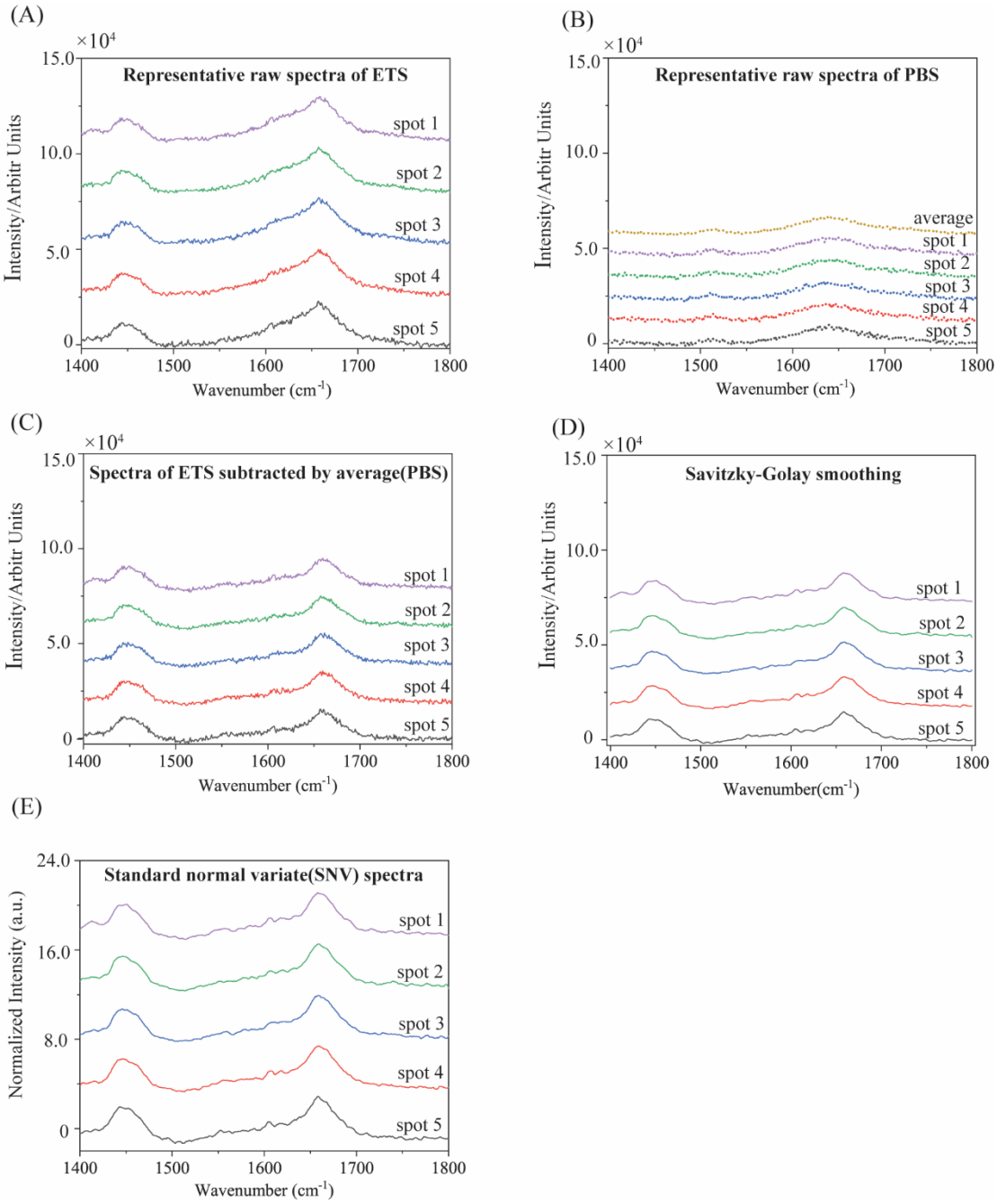

Figure 5. The preprocessing steps are performed sequentially to the representative spectra (only five spectra shown for clarity). (A) The representative- raw spectra of ETS sample for spot 1 to spot 5 (five scanning locations) and (B) the spectra of PBS buffer for spot 1 to spot 5 plus averaged spectra of PBS for five locations after trimming to the region between 1400-1800 cm^{-1}. (C) The spectra of ETS sample were subtracted from averaged PBS buffer. (D) The spectra were smoothed by a Savitzky-Golay filter with a window size of 11 and a 3rd order polynomial and (E) the spectra were normalized by standard normal variate (SNV) transformation.

The objective of PCA analysis is to perceive the relationship between the intensity variation and sample alignment. This is hard to achieve by using a single variable (e.g., intensity at a given wavenumber) because one specific variable could be influenced by multiple experimental factors (e.g., sample groups, environment, measurement conditions). This makes it difficult to correlate to one single factor while eliminating the effect of all other factors. Besides, one experimental factor can impact multiple variables (e.g., intensities at multiple wavenumbers). For example, multiple intensities can change with sample alignment. This complexity motivates us to use a multivariate analysis, which can deal with more than one variable at a time and help find the key variables (e.g., intensities of different wavenumbers) related to the factor under consideration. In order to relate intensity variations from different polarized angels to alignment state, spectra from the sample of known alignment state have been used to train the multivariate PCA model. Here, we used a trained PCA model from highly aligned native muscle tissue as previously described,[17] which relates variations of the intensities of key Raman bands to the degree of alignment in tissue. This PCA training model derives a master loading function, which transformed hundreds of intensities into a single variable called PC1 Score for better visualization of the trends in the dataset (Fig. 4). This transformation can be implemented in MATLAB® for a given dataset (see Appendix S2). There are two reasons for using this muscle-derived loading function. First, this loading captures the most important Raman bands related to matrix alignment from the canonical model of highly aligned matrix containing in native muscle. Second, the matrix composition in native muscle is similar to that in ETS, including collagen (type I, III and IV), glycoproteins (fibronectin and laminin), proteoglycans, glucosaminoglycans and elastins.[26–28] Then PC1 Score as a function of polarized angle was fitted with a sine function , in which the amplitude indicates the degree of alignment in tissue (see equation S1).

The sine fitting can be performed in Origin software (OriginLab, Northampton, MA, USA), and the fitting details and parameters can be seen in Appendix S1B and Table S2. The fitting can be carried out for one sample location and then can be operated via batch processing tool in the Origin for a dataset of 22 points. Our hypothesis is that a single metric-amplitude can distinguish the different alignments in ETS. Therefore, the spectra of ETS samples of all seven polarized angles were implemented via PCA and the amplitude for each sample location could be obtained.

4. Alignment characterization by microscopy imaging

To compare the alignment results by PRS method with that from the traditional microscope method, additional ETS samples were prepared in the same way as for Raman spectroscopy. Then fixed engineered scaffolds were incubated in 5% Bovine Serum Albumin diluted in PBS for 30 min at room temperature to block non-specific background in fixed cells. To label the cell and ECM components in ETS samples, the scaffolds were rinsed in PBS several times and fluorescently labeled by Alexa Fluor™ 488 N-Hydroxysuccinimide (NHS) ester (diluted 1:500), Alexa Fluor™ 4,6-diamidino-2-phenylindole (DAPI) (diluted 1:500), and Alexa Fluor™ phalloidin (diluted 1:200) for at least 30 min in a dark room. Then ETS samples were washed for extended time with PBS and mounted on glass slides using mounting media. Scaffold morphology was examined using a Keyence inverted microscope (Keyence BZ-X810; Keyence Corporation, Itasca, IL, USA) through 20X objective (NA= 0.6, S Plan Fluor ELWD ADM 20XC, Nikon, EI Segundo, CA, USA) with a 200X total magnification. This can provide a field view size of 725 μm×544 μm with an image resolution of 0.3744 μm per pixel.

For image analysis, an open-source software CT-FIRE was used to (freely available at https://eliceirilab.org/software/ctfire/) extract individual fibers from immunofluorescence images of ETS and obtain orientation histogram of the matrix fibers. First, an original image is opened and automatically becomes binary image in CT-FIRE (Fig. 6a and 6b). 11 ROIs are selected for analysis (Fig. 6c) to obtain the orientation histogram of detected fibers in each ROI (Fig. 6d). Briefly, a threshold is set for analysis by selecting fiber extraction parameter "thresh_im2" (Fig. 6e). This parameter is set to 20 so that foreground pixels represent potential fibers and background pixels represent pixels where no fiber is present in CT-FIRE software. Meanwhile, "overlaid fiber" and "Angle histogram and values" are boxed for showing the images of detected fibers and obtaining the angular distribution of the fibers, respectively (Fig. 6f). Then run "manager ROI" to select 11 ROIs (each ROI: 53.4 pixels by 53.4 pixels=$20\mu m \times 20\mu$m) for each image, considering the image resolution is 2.67 pixels/μm (Fig. 6g). This analysis ROI is the same dimension for PRS measurement on ETS for 2 ROIs in total (20 μm). Afterwards, run "apply ctFIRE analysis on ROI" to obtain angular distribution of individual fibers for each ROI. The histogram files containing the angles of individual fibers in a single column were saved as "HistAng_ctFIRE_xxx (image name).csv" by default. The Image Alignment Index (IAI) was calculated based on angle distribution in each histogram file by performing a previously described method [29] and the calculation can be performed in MATLAB using the equation below:

$$Image\ alignment\ index = 2 \times \frac{\int_0^\pi N(\alpha) cos^2\alpha\ d\alpha}{\int_0^\pi N(\alpha)\ d\alpha} - 1 \quad (4)$$

where α is orientation angle between an individual fiber and the mean axis of all the fibers and N(α) is the number of fibers oriented at the angle α. The integration spans from 0 to π due to symmetry orientation of fibers.

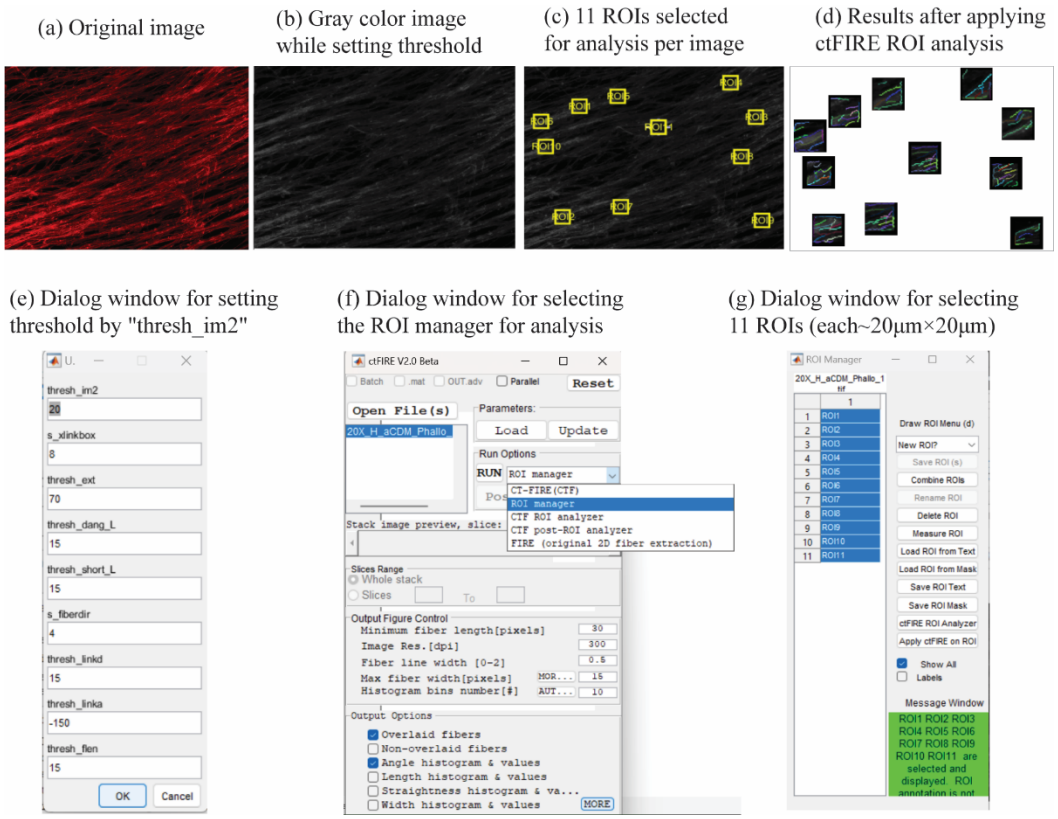

Figure. 6 The process of image analysis. (a) the original image of fluorescently labeled F-actin protein as an example. (b) gray color image of the original image while setting threshold for detecting the fibers in the image and (c) 11 ROIs were selected for fiber angular distribution analysis. (d) Results after applying ctFIRE on ROI showing the images of overlaid detected fibers for 11 ROIs and (g) corresponding dialog window showing 11 ROIs built and selected. And the corresponding working dialog windows. (e) for setting by "thresh_im2" parameter to 20, (f) for analysis by selecting "ROI manager" and boxing "overlaid fibers" and "Angle histogram and values" and (g) for selecting 11 ROIs.

5. Statistical analysis.

The unequal variance tests (including O'Brien, Brown-Forsythe, Levene, Bartlett and F Test 2-sided) were used to test if the variances of Amplitude Alignment Metric (AAM) or Image Alignment Index (IAI) between two groups (aETS and iETS) are equal by choosing "UnEqual Variances" in JMP statistical software (SAS company, Cary, NC, USA). If unequal test passed (i.e., if any of five statistical tests mentioned here is significant, p <0.05), then unequal variances t-test (two-sample) would be used to evaluate if the means of these alignment indices between

aETS and iETS have significant differences, otherwise a pooled two-sample student *t*-test was used. All the *t*-tests were performed with a confidence level of 0.95. The unequal variances *t*-test started with estimating the difference between the population means for the two groups, then calculated the pooled standard deviation adjusted for group size and finally obtained the test statistics by the ratio of difference of average and standard error of difference. Statistical *p*-values and tables about estimation of standard deviation and variance are calculated accordingly by using *t*-test command for unequal variances *t*-test. All graphs and statistical computations can be performed in the "Distribution" and "Fit Y by X" platforms of the Analyze menu in JMP. In this work, unequal variances *t*-test (two-sample) was performed for AAM and IAI of ester fluorescence images and phalloidin fluorescence images under the assumption of unequal variance. The two-sample pooled student *t* test was used for R^2 of sine fittings for PC1 Score under the assumption of equal variance. Probability > |*t*| was used to indicate *p*-value if the means of alignment indices or R^2 have significant differences ($\mu T \neq \mu C$).

Results and Discussions

22 spectra from 22 locations in ETS per polarized angle were obtained (Fig. 7A) and then sequentially preprocessed by subtracting PBS background averaged from five locations, smoothing using 3rd polynomial and window size of 11 and SNV normalization as mentioned in the previous section. Then the same preprocessing was repeated for the datasets of another six polarized angles. The mean Raman spectrum of all polarized angles for each sample was shown in Fig. 7B. All native muscle and engineered tissues (aETS and iETS) contain similar Raman bands such as CH_2 bending band, CH_2/CH_3 deformation, C=C stretching, C=O stretching that were assigned to lipids and carbohydrates, collagen and lipids, amino acids (e.g., tryptophan,

phenylalanine, etc.) and proteins, respectively (Table 1). For polarized Raman scattering light, greater intensities among different directions (different polarized angles) means greater anisotropy of Raman signal, which is a result of higher structural anisotropy in samples. PCA defines a loading function, assigning weights for Raman bands as their contribution to directional-dependent difference of the Raman spectra. Here, muscle-trained loading function was used due to similar biochemical composition between native muscle and engineered tissue (Table 1). In this muscle loading function, the large magnitude of weights (~10%-20%) for different Raman bands (e.g., 1444 cm^{-1}, 1465 cm^{-1}, 1605 cm^{-1}, 1627-1660 cm^{-1} and 1665-1689 cm^{-1}) indicates a strong correlation of those Raman bands to alignment (Fig. 7C). After the linear combination of Raman intensities and weights in the loading function, PC1 Score was obtained for each polarized angle per sample location. To relate the variations of PC1 Score to alignment, the PC1 Score as a function of polarized angle was fitted with sine function to quantify the degree of variation along different polarized angles. For each location, a sine fitting was obtained and the R^2 was calculated for the fitting. Unequal variance test showed equal variance between two groups (aETS vs iETS) since all five tests (Bartlett's test, Brown-Forsythe test, Levene test, Bartlett and F Test 2-sided) passed at significant level of 0.05, as shown in Table 2. Therefore, a pooled student *t* test was performed, and the results are shown in Table 3. In Fig. 7D and 7E, the aETS yields a greater R^2 of sine fits compared to the iETS ($p < 0.0001$ using two-sample pooled student *t*-test) and raw data about R^2 can be found in Table S3. We also found some poor sine fits of iETS approaching a flat line (zero amplitude or a constant value) while sine fits of aETS did not. These data indicate that sine fits reasonably captured variations in Raman intensities that may be related to aligned matrix in aETS while iETS showed random variations that sine fits failed to capture.

Table 1. Wavenumber values of Raman bands and tentative assignment for ETS and muscle

Tentative Assignment	Raman band (cm^{-1})			Refs
	Native muscle	aETS	iETS	
CH_2 bending (lipids, carbohydrates, etc.)	1450	1448	1452	30
CH_2/CH_3 deformation (collagen &lipids)	1463	1461	1463	31
Tryptophan, ν(C=C) (proteins)	1553	1553	1563	32
Phenylalanine, hydroxyproline (proteins)	1586	1586	1587	31
Phenylalanine, tyrosine, δ(C=C) (proteins)	1605	1605	1605	33
Tyrosine, tryptophan, ν(C=C) (proteins)	1616	1617	-	34
Amide I, ν(C=O) (proteins)	1653, 1667	1658, 1668	1633, 1665	35

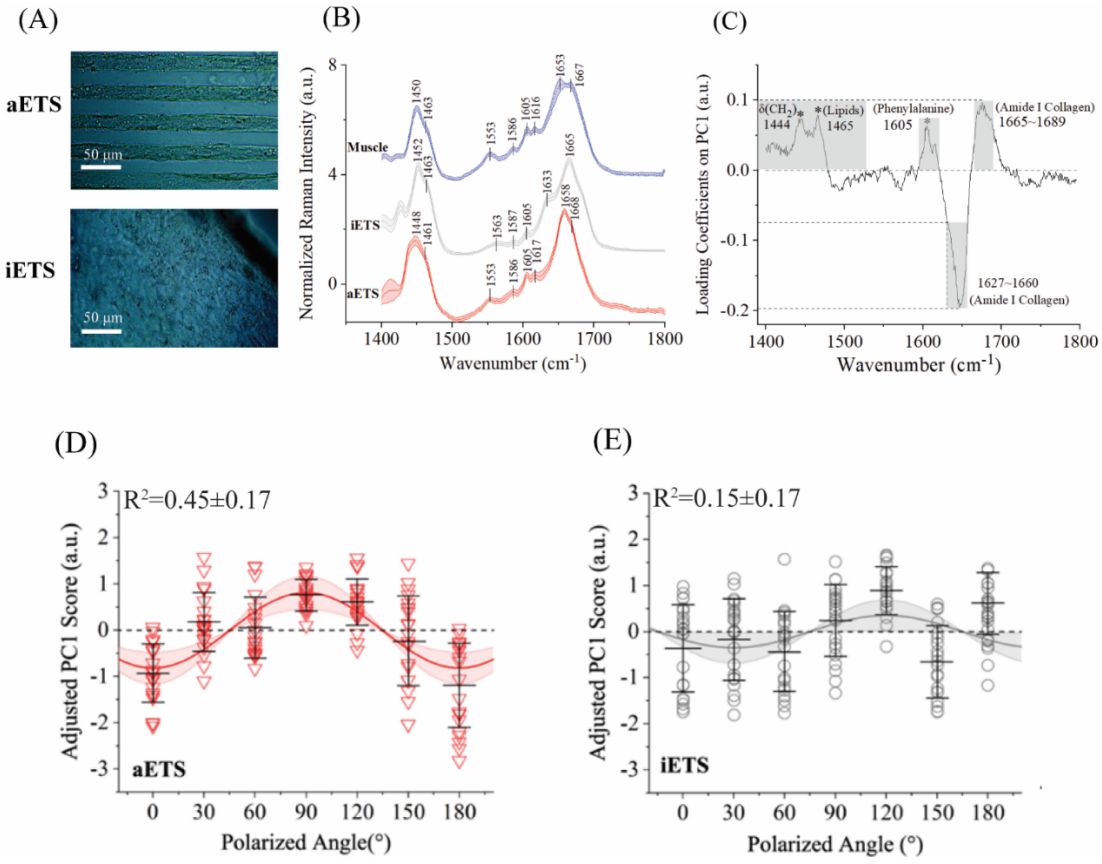

Figure 7. Applying muscle derived loading function to spectra of ETS shows better sine fitting for aETS as compared to iETS. (A) Bright field images of ETS samples for PRS measurement in the 0˚ polarization configuration and definition of polarization angle (lower panel). (B) Raman

spectra (n = 147 technical replicates) of native muscle, aETS and iETS in the 1400-1800 cm^{-1} range. Solid lines represent standard normal variate (SNV) normalized mean spectra and shaded areas represent corresponding standard deviation. (C) Principal component loading curve for primary principal component (PC1) was derived based on native muscle spectra (110 spectra total). Bands in the loading curve correspond to CH_2, lipids, phenylalanine and Amide I vibration modes, respectively, which are known to be present in both native soft tissue and engineered scaffolds. PC1 Score for (D) aETS yields a reasonable sine fit whereas PC1 Score for (E) iETS yields a poor sine fit. PC1 Score is fitted by the sine function. PC1 Scores and sine fits are shifted by y_0 for clarity. Solid line refers to the mean of all sine fits (n=21 technical replicates) and shaded areas represent corresponding standard deviation. Error bars indicate one standard deviation of the mean of PC1 Score per angle. R^2 = Goodness of fit value for sine fit. The averaged R^2 =0.45 for aETS and averaged R^2=0.15 for iETS.

Table 2. Statistical table of unequal variance test for R^2 of sine fittings

Test	*F*-ratio	Df (numerator)	Df (denominator)	*p*-value
O'Brien test	4.9899	1	85	0.9645
Brown-Forsythe	3.9877	1	85	0.7712
Levene	5.3359	1	85	1.0000
Bartlett	6.4801	1		0.9553
F-Test 2-sided	2.2133	42	43	0.9553

Note: *F*-ratio is calculated from *F*-statistic. Df (numerator) and Df (denominator) refer to the degrees of freedom in the numerator and denominator, respectively. *p*-value indicates the probability of obtaining an *F*-ratio value larger than the one calculated if the variances are equal across all levels.

Table 3. Statistics of two-sample pooled student *t*-test for R^2 (confident level=0.95)

Statistics	Values
Difference in mean values of groups	-0.30095
Std Error of the difference	0.05288
Upper confidence limit for the difference	-0.19409
Lower confidence limit for the difference	-0.40782
t-ratio*	-5.69171
Degree of freedom	40
Prob >|*t*|	< 0.0001

**t*-ratio is calculated as the ratio of the difference in group means over the pooled standard error of both groups in the *t*-statistic. Pro>|*t*| is the *p*-value associated with a two-tailed test (null hypothesis: $\mu T \neq \mu C$).

We calculated the AAM for each sample point and compared the mean values between aETS and iETS groups. Before the *t*-test, the variances of two populations of AAM were tested

(hypothesis: $\sigma_1^2 \neq \sigma_2^2$) based on *F*-statistics by calculating a ratio of the mean square between groups divided by a mean square within groups (called *F*-ratio). In this case, *F*-ratios for all five tests were larger than 1, indicating the null hypothesis is rejected (Table 4). Meanwhile, the *p*-values for Bartlett's test, Brown-Forsythe test, Levene test, Bartlett and F Test 2-sided were all less than 0.05, indicating the variability in the amplitude values for aETS is significantly different than that for the iETS (Table 4). Due to unequal variance between aETS and iETS groups, an unequal variances *t*-test was performed instead of the pooled two-sample *t*-test and the detailed statistical values are shown in Table 5. The calculated *t*-statistics was -4.28013 and the *p*-value was smaller than 0.0001 after checking the *t*-distribution with a specific degree of freedom and a chosen alpha value (α=0.05). While aETS may consist of slightly different matrix composition as compared to iETS, we were still able to distinguish structural anisotropy vs isotropy in the ETS samples due to a significantly higher AAM of aETS than iETS (see Fig. 8). Although the mean of the AAM for aETS (~0.8) is smaller than the same metric we measured in native muscle previously (~1.1),[17] a degree of anisotropy is still developed in engineered tissue with cells cultured on patterned PDMS. The variability of this AAM for ETS samples (~20%) may be reflected as the heterogeneity assembled by cells at molecular level, considering Raman spectral intensities rely on molecular vibrations. This PRS alignment for aETS is contributed by protein (amide I), lipids, phenylalanine and carbohydrates (CH_2) in scaffolds, indicating the heterogenous network of these macromolecules for just 2-week cell remodeling. The different degrees of microscale anisotropy between engineered tissue and native tissue indicated by this AAM may help explain the low mechanical strength of engineered scaffolds as compared to native tissue.

Table 4. Statistical table of unequal Variance test for Amplitude Alignment Metric

Test	F ratio	Df (numerator)	Df (denominator)	*p*-value
O'Brien test	4.9899	1	85	*0.0281
Brown-Forsythe	3.9877	1	85	*0.0490
Levene	5.3359	1	85	*0.0233
Bartlett	6.4801	1		*0.0109
F-Test 2-sided	2.2133	42	43	*0.0109

Note: *F*-ratio is calculated from *F* statistic. Df (numerator) and Df (denominator) refer to the degrees of freedom in the numerator and denominator, respectively. *p*-value indicates the probability of obtaining an *F*-ratio value larger than the one calculated if the variances are equal across all levels. The symbol * indicates the statistical test passed at $p < 0.05$.

Table 5. Statistics of two-sample *t*-test for Amplitude Alignment Metric (confident level=0.95)

Statistics	Values
Difference in mean values of groups	-0.39731
Std Error of the difference	0.09283
Upper confidence limit for the difference	-0.01528
Lower confidence limit for the difference	-0.77935
t-ratio*	-4.28013
Degree of freedom	73.31624
Prob >|*t*|	< 0.0001

**t*-ratio is calculated as the ratio of the difference in group means over the pooled standard error of both groups in the *t*-statistic. Pro>|*t*| is the *p*-value associated with a two-tailed test (null hypothesis: $\mu T \neq \mu C$).

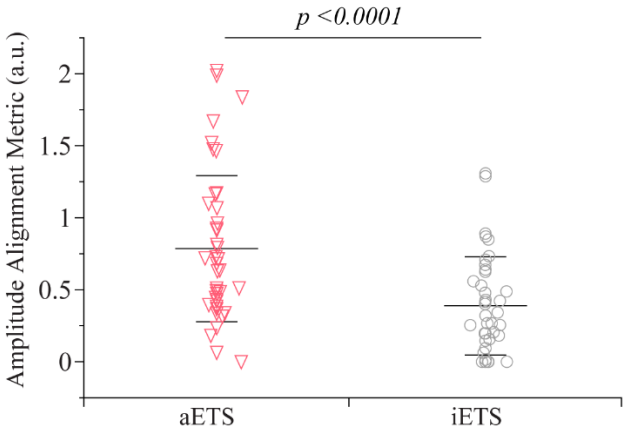

Figure 8. PRS analysis distinguished anisotropy and isotropy in ETS. The Amplitude Alignment Metric calculated by amplitude analysis of PC1 scores is significantly higher for aETS than iETS (0.785 ± 0.507 versus 0.388 ± 0.341, Mean ± SD) as determined by the two-tailed two sample *t* test (n=43 technical replicates for aETS and n=44 technical replicates for iETS). Horizontal lines indicate mean and standard deviation.

Furthermore, PRS alignment metric was compared to an image index calculated from the detected fibers in the immunofluorescence (IF) images. For immunofluorescence, dyes functionalized with NHS ester groups that covalently couple amine-containing biomolecules (e.g., proteins and peptides) can label all the proteins in ETS whether they are matured or not. Phalloidin was used to label intracellular protein F-actin. Protein fibers in aETS were shown to be aligned along the microchannel direction for all matrix proteins (Fig. 9A) and for F-actin (Fig. 10A). For iETS, the protein fibers including total matrix proteins and intracellular proteins were randomly oriented in all the directions (Fig. 9B and Fig. 10B). To further quantify the degree of alignment by immunofluorescence microscopy method and compare it to PRS method, 11 microscopic ROIs (20μm × 20 μm) were selected on each IF image for analysis, which is the dimension for Raman ROIs measured on ETS for 2ROIs in total (20 μm). An Image Alignment Index (IAI) was calculated based on the averaged square cosine of all fiber orientation angles for each ROI as mentioned in the previous method section. The IAI is equal to 1 implying perfect alignment while being equal to 0 means random orientation. Besides, the mesoscale alignment was also quantified using the same method as microscopic alignment for the whole image frame of larger size (725μm × 544 μm) and the orientation angles of detected fibers were plotted as polar orientation histogram shown in Fig. 9E and Fig. 9F. While aETS shows global anisotropy shown in Fig. 9E and Fig. 10E, protein fibers can be highly aligned or less aligned (Fig. 9C and Fig. 10C) locally for microscopic ROIs with higher IAI or lower IAI. Similarly, while iETS displays global isotropy shown in Fig. 9F and Fig. 10F, it also shows heterogeneity with some local alignment (Fig. 9D and Fig. 10D). To compare microscopic alignment by immuofluorence microscopy method to PRS method, the image-processing-based alignment index was quantified based on IF images for matrix proteins and for intracellular proteins as mentioned in the Method

section. The IAI was calculated for each ROI and the statistics of the index were calculated based on the same sample size per tissue type (n=43-44) as that of PRS data. By performing unequal variances *t*-test on IAI for ester and phalloidin, two tests (Bartlett and *F*-Test 2-sided) showed *p*-value smaller than 0.05 for ester and all five tests showed *p*-value smaller than 0.05 for phalloidin (Table 6). All these indicate the variance for IAI for both proteins were significantly unequal and two-sample *t*-test should be used. The calculated *t*-statistic was -3.27559 and -2.7445 for ester and phalloidin, respectively, corresponding to the p-value of 0.0016 and 0.0076 after checking the *t*-distribution with a specific degree of freedom and a chosen alpha value (α=0.05) as shown in Table 7. Hence, the resulting *p*-values were larger than those obtained for our PRS-based method (see Table 3 and Table 5), indicating a greater differentiating capacity for tissue anisotropy at microscale via the PRS-based method compared to microscopy method. Similar to PRS-based alignment metric, a significantly higher mean of alignment of aETS than iETS was observed for both matrix proteins (Fig. 11A) and intracellular proteins (Fig. 11B). We also compared the variability of the PRS-based AAM with the variability of IAI. The variability of PRS-based alignments (averaged ~21%) was similar to the variability of IAI for all the labeled matrices (averaged~20%). Each method has its own advantages and drawbacks. The immunofluorescence microscopy can directly visualize the mesoscale architecture in tissue but requires labeling. For microscopic alignment, the errors for quantifying local alignment in image analysis can be high due to a low number of fibers per frame. This feature-based image analysis on protein fiber alignment can be easily impacted by the resolution of images and quality of images, which is determined by the sample state (e.g., thickness, transparency, etc.). Although increasing magnification can embrace more details at microscopic level, the image quality can be worse at high magnification as compared that at low magnification when the sample is thick or

not flat. Hence, a better discriminatory capacity was observed towards tissue anisotropy at microscale by PRS method than microscopy image method in this study. Microscopic alignment for fibers and even smaller fibrils were very important and basic elements contributing to overall properties of engineered constructs (e.g., mechanical properties), which is hard to see by microscopy at molecular level. The PRS method can serve as complementary tool to monitor microscopic alignment at molecular level of biomacromolecules in engineered tissue in a label-free manner with minimal preparation. However, the variability of PRS-based AAM may limit the ability of this technique to discern intermediate cases where ECM is partially aligned. Nevertheless, it can be especially useful for tissue engineers hoping to obtain highly aligned engineered tissues, such as musculoskeletal (muscle, cartilage and ligament), cardiac muscle, etc. This can be true due to the capability of providing a useful suggestion like “stopping point” for *in vitro* conditioning of initially unaligned tissue based on their demonstrated level of alignment. Moreover, PRS characterization on fresh tissue was also studied, no significant difference of PC1 Score between fresh tissue and processed tissue was observed (Fig. S4). Although the minimal effect of chemical processing on tissue, this PRS method has potential to monitor alignment in live engineered tissue scaffolds without labels or any processing. Overall, these established protocols can help guide future experiments for monitoring the microscopic alignment over a larger area and such alignment in live engineered tissue.

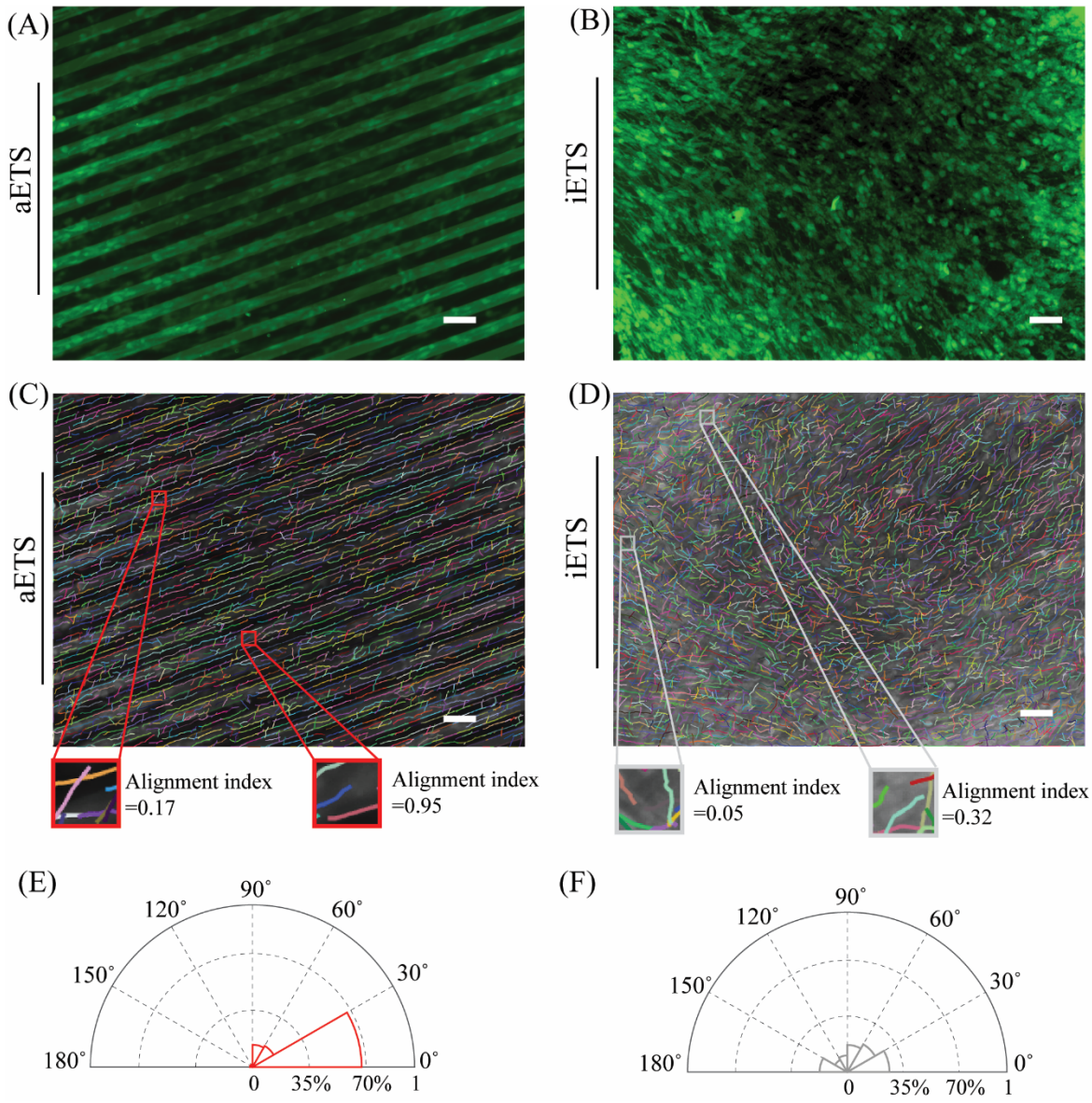

Figure 9. The quantified alignment at microscopic scale (20μm× 20μm) and mesoscale (725μm× 544μm) from immunlfuoresnce images of labeled total proteins in ETS. (A) The original immfuluoresnce images of total proteins for aETS and (B)iETS. Images of CT-FIRE segmented fibers indicated by colored lines overlaid on the top of grey color original IF images for (C)aETS and (d)iETS. In each sub figure, two insets indicate zoomed-in views of two boxed ROIs (20 μm×20 μm)on each CT-FIRE map, where one displays a relatively high degree of matrix alignment and the other shows a relatively low degree of matrix alignment. The corresponding polar orientation histogram of all detected fibers in each CT-FIRE map for the whole image frame for (E) aETS and (F) iETS. Scale bar: 50 μm

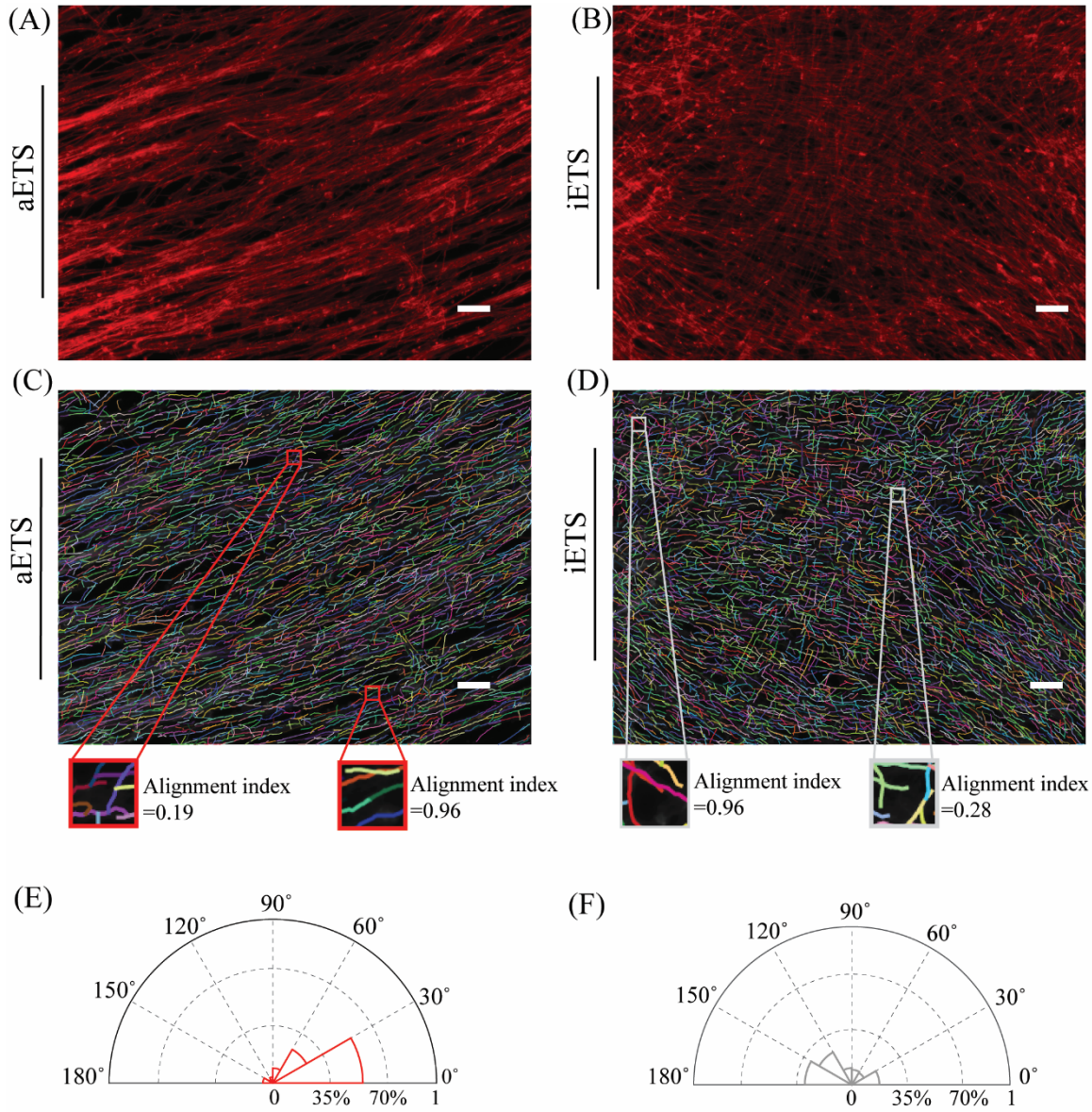

Figure 10. The quantified alignment at microscopic scale (20μm× 20μm) and mesoscale (725μm× 544μm) from immunlfuoresnce images of labeled F-actin of ETS. (A) The original immfuluoresnce images of F-actin for aETS and (B)iETS. Images of CT-FIRE segmented fibers indicated by colored lines overlaid on the top of grey color orignal IF images for (C)aETS and (d)iETS. In each sub figure, two insets indicate zoomed-in views of two boxed ROIs (20 μm×20 μm)on each CT-FIRE map, where one displays a relatively high degree of matrix alignment and the other shows a relatively low degree of matrix alignment. The corresponding polar orientation histogram of all detected fibers in each CT-FIRE map for the whole image frame for (E) aETS and (F) iETS. Scale bar: 50 μm

Table 6. Statistical table of unequal variance test for Image Alignment Index

Test	F ratio	Df (numerator)	Df (denominator)	*p*-value
		Image Alignment Index (ester)		
O'Brien test	2.3190	1	86	0.1315
Brown-Forsythe	2.4693	1	86	0.1198
Levene	2.2441	1	86	0.1378
Bartlett	7.1558	1		*0.0075
F-Test 2-sided	2.2927	42	44	*0.0074
		Image Alignment Index (phalloidin)		
O'Brien test	4.4324	1	86	*0.0382
Brown-Forsythe	4.8832	1	86	*0.0298
Levene	7.0954	1	86	*0.0092
Bartlett	6.8247	1		*0.0090
F-Test 2-sided	2.2476	42	44	*0.0089

Table 7. Statistics of two-sample *t*-test for Image Alignment Index (confidence level= 0.95)

Image Alignment Index (ester)		Image Alignment Index (phalloidin)	
Statistics	**Values**	**Statistics**	**Values**
Difference	-0.10784	Difference	-0.14843
Std Error difference	0.03292	Std Error difference	0.05408
Upper CL difference	-0.04222	Upper CL difference	-0.04064
Lower CL difference	-0.17347	Lower CL difference	-0.25622
t-ratio	-3.27559	*t*-ratio	-2.7445
Degree of freedom	72.31431	Degree of freedom	72.75165
Prob >|*t*|	0.0016	Prob >|*t*|	0.0076

Note: Difference means the estimated difference between the two-group means. Std error difference is the standard error of the difference. Upper CL difference is the upper confidence limit for the difference. Lower CL difference refers to the lower confidence limit for the difference. *t*-ratio is calculated as the ratio of the difference in group means over the pooled standard error of both groups in the *t*-statistic.

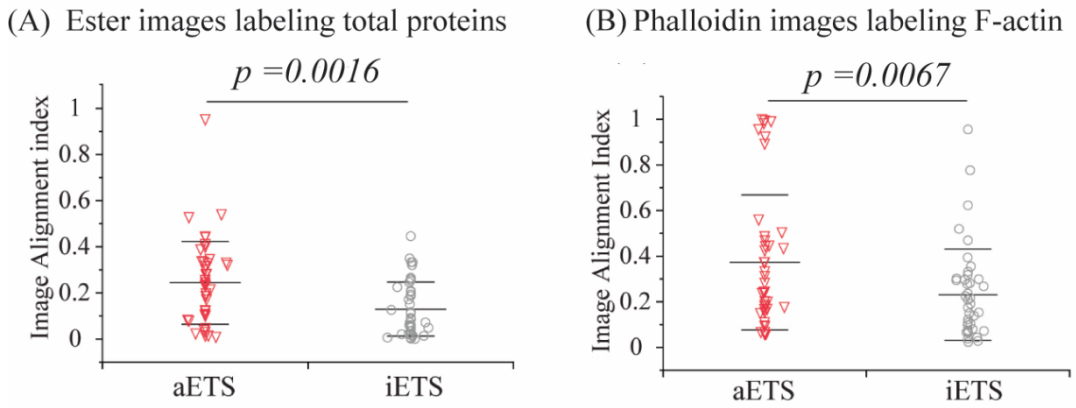

Figure 11. Quantification of Image Alignment Index (IAI) via analysis of orientation histogram of CT-FIRE segmented fibers in the IF images of (A) ester and (B) phalloidin. A significantly higher IAI was shown in aETS(0.244 ± 0.180) than iETS (0.129 ± 0.117) for matrix protein and in aETS (0.373 ± 0.295) than iETS (0.231 ± 0.200) for intercellular protein. N=44 technical replicates for each tissue group. Scale bar: 50 μm

Conclusions

The PRS-based platform was successfully used to distinguish anisotropy (aligned) versus isotropy (unaligned) at molecular level in engineered tissue scaffolds of varying matrix components. Coupling with PCA training function from native aligned tissue, complex Raman spectra can be simplified into one simple variable PC1 Score that can be related to the degree of alignment from various matrix components in ETS, including common biomacromolecules (protein, lipids and carbohydrates) in engineered tissue. Eventually, the degree of alignment for complex matrix can be quantified as a simple index (AAM) that can be used to compare across different engineered tissue samples. The mean of this metric was shown to be significantly higher for aETS (anisotropic) than iETS (isotropic), implying the ability to successfully distinguish the alignment in engineered tissues. Although the variability of PRS-based AAM was similar to the Image Alignment Index (IAI) for ETS samples, the distinguishing capacity of micro-region anisotropy was higher for AAM as revealed by a smaller *p*-value of PRS metric (*p*-value (AAM)<0.0001 vs *p*-value (IAI)<0.002). Hence the established PRS-based alignment metric has the potential to monitor alignment of complex matrix at molecular level in engineered tissues and hence can support tissue engineers in mimicking the mechanical properties of native tissues with organized, hierarchical protein structures in a label-free manner.

ASSOCIATED CONTENT

Supporting Information Available

The following files are available free of charge:

Figures S1-S4 showing the phase contrast images of aETSs and iETS, the bright field image of ETS samples before PRS measurement, the polynomial fitting for subtracting fluorescence background from Raman spectra and Raman spectra between native muscle and engineered tissue scaffolds, respectively; Table S1-S4 with the parameters set for PRS measurement and sine fitting, plus statistical values for unequal test and two-sample *t* test. Appendix S1 contains additional notes of methods for preparation of cardiac fibroblasts, PBS data acquisition and analysis, PRS characterization, sine fitting and amplitude caculation, immunofluorescence imaging; Appendix S2 contains MATLAB routine for Preprocessing and PCA analysis (PDF). Two text files for raw Raman spectra of ETS from spot 1 to spot 5 and raw Raman spectra of PBS from spot 1 to spot 5.

Corresponding Author

*Tel: 1 352-727-8662. Email: subhash@ufl.edu

ACKNOWLEDGMENTS

The authors acknowledge support from the National Science Foundation (CMMI 1762791) and the Army Research Office (DURIP Instrumentation Grant ARO-68410-EG-RIP). We also thank Dr. Sharon Karackattu for her assistance with experiments.

REFERENCES

(1) Thomopoulos, S.; Fomovsky, G. M.; Holmes, J. W. The Development of Structural and Mechanical Anisotropy in Fibroblast Populated Collagen Gels. *J. Biomech. Eng.* **2005**, *127* (5). https://doi.org/10.1115/1.1992525.

(2) Middendorf, J. M.; Griffin, D. J.; Shortkroff, S.; Dugopolski, C.; Kennedy, S.; Siemiatkoski, J.; Cohen, I.; Bonassar, L. J. Mechanical Properties and Structure-Function Relationships of Human Chondrocyte-Seeded Cartilage Constructs after in Vitro Culture. *J. Orthop. Res.* **2017**, *35* (10), 2298–2306. https://doi.org/10.1002/jor.23535.

(3) Zhang, S.; Singh, S.; Winkelstein, B. A. Collagen Organization Regulates Stretch-Initiated Pain-Related Neuronal Signals in Vitro: Implications for Structure–Function Relationships

in Innervated Ligaments. *J. Orthop. Res.* **2018**, *36* (2), 770–777. https://doi.org/10.1002/jor.23657.
(4) Win, Z.; Vrla, G. D.; Steucke, K. E.; Sevcik, E. N.; Hald, E. S.; Alford, P. W. Smooth Muscle Architecture within Cell-Dense Vascular Tissues Influences Functional Contractility. *Integr. Biol. (United Kingdom)* **2014**, *6* (12), 1201–1210. https://doi.org/10.1039/c4ib00193a.
(5) Catros, S.; Guillemot, F.; Nandakumar, A.; Ziane, S.; Moroni, L.; Habibovic, P.; Van Blitterswijk, C.; Rousseau, B.; Chassande, O.; Amédée, J.; Fricain, J. C. Layer-by-Layer Tissue Microfabrication Supports Cell Proliferation in Vitro and in Vivo. *Tissue Eng. - Part C Methods* **2012**, *18* (1), 62–70. https://doi.org/10.1089/ten.tec.2011.0382.
(6) Sjoerd Van Helvert, C. S. and; Friedl, P. Mechanoreciprocity in Cell Migration. *Nat. Cell Biol.* **2018**, *20*, 8–20. https://doi.org/10.1038/s41556-017-0012-0.
(7) Fraley, S. I.; Wu, P.; He, L.; Yunfeng Feng, Ranjini Krisnamurthy, G. D. L. and D. W. Three-Dimensional Matrix Fiber Alignment Modulates Cell Migration and MT1-MMP Utility by Spatially and Temporally Directing Protrusions. *Sci. Rep.* **2015**, *5*, 14580. https://doi.org/10.1038/srep14580.
(8) Joseph A. Madri, B. M. P. and A. M. T. Phenotypic Modulation of Endothelial Cells by Transforming Growth Factor-β Depends upon the Composition and Organization of the Extracellular Matrix. *J. Cell Biol.* **1988**, *106*, 1375–1384.
(9) Reilly, G. C.; Engler, A. J. Intrinsic Extracellular Matrix Properties Regulate Stem Cell Differentiation. *J. Biomech.* **2010**, *43* (1), 55–62. https://doi.org/10.1016/j.jbiomech.2009.09.009.
(10) Xu, R.; Boudreau, A.; Bissell, M. J. Tissue Architecture and Function: Dynamic Reciprocity via Extra- and Intra-Cellular Matrices. *Cancer Metastasis Rev.* **2009**, *28* (1–2), 167–176. https://doi.org/10.1007/s10555-008-9178-z.
(11) Bissell, C. M. N. and M. J. Of Extracellular Matrix , Scaffolds, and Signaling : Tissue Architecture Regulates Development , Homeostasis, and Cancer. *Annu. Rev. Cell Dev. Biol.* **2006**, *22*, 287–309. https://doi.org/10.1146/annurev.cellbio.22.010305.104315.
(12) Chen, X.; Nadiarynkh, O.; Plotnikov, S.; Campagnola, P. J. Second Harmonic Generation Microscopy for Quantitative Analysis of Collagen Fibrillar Structure. *Nat. Protoc.* **2012**, *7* (4), 654–669. https://doi.org/10.1038/nprot.2012.009.
(13) Wolman, M.; Kasten, F. H. Polarized Light Microscopy in the Study of the Molecular Structure of Collagen and Reticulin. *Histochemistry* **1986**, *85* (1), 41–49. https://doi.org/10.1007/BF00508652.
(14) Butler, H. J.; Ashton, L.; Bird, B.; Cinque, G.; Curtis, K.; Dorney, J.; Esmonde-White, K.; Fullwood, N. J.; Gardner, B.; Martin-Hirsch, P. L.; Walsh, M. J.; McAinsh, M. R.; Stone, N.; Martin, F. L. Using Raman Spectroscopy to Characterize Biological Materials. *Nat. Protoc.* **2016**, *11* (4), 664–687. https://doi.org/10.1038/nprot.2016.036.
(15) Zhou, H.; Simmons, C. S.; Sarntinoranont, M.; Subhash, G. Raman Spectroscopy Methods to Characterize the Mechanical Response of Soft Biomaterials. *Biomacromolecules* **2020**, *21* (9), 3485–3497. https://doi.org/10.1021/acs.biomac.0c00818.
(16) Matthew J Baker, Júlio Trevisan, Paul Bassan, Rohit Bhargava, Holly J Butler, Konrad M Dorling, Peter R Fielden, Simon W Fogarty, Nigel J Fullwood, Kelly A Heys, Caryn Hughes, Peter Lasch, Pierre L Martin-Hirsch, Blessing Obinaju,, Ganesh D Sockalingum, J, and F. L. M. Using Fourier Transform IR Spectroscopy to Analyze Biological Materials. *Nat. Protoc.* **2014**, *9* (8), 1771–1791.

https://doi.org/10.1038/nprot.2014.110.Using.
(17) Zhou, H.; Piñeiro Llanes, J.; Sarntinoranont, M.; Subhash, G.; Simmons, C. S. Label-Free Quantification of Soft Tissue Alignment by Polarized Raman Spectroscopy. *Acta Biomater.* **2021**, *136*, 363–374. https://doi.org/10.1016/j.actbio.2021.09.015.
(18) Galvis, L.; Dunlop, J. W. C.; Duda, G.; Fratzl, P.; Masic, A. Polarized Raman Anisotropic Response of Collagen in Tendon: Towards 3D Orientation Mapping of Collagen in Tissues. *PLoS One* **2013**, *8* (5), 1–9. https://doi.org/10.1371/journal.pone.0063518.
(19) Masic, A.; Bertinetti, L.; Schuetz, R.; Galvis, L.; Timofeeva, N.; Dunlop, J. W. C.; Seto, J.; Hartmann, M. A.; Fratzl, P. Observations of Multiscale, Stress-Induced Changes of Collagen Orientation in Tendon by Polarized Raman Spectroscopy. *Biomacromolecules* **2011**, *12* (11), 3989–3996. https://doi.org/10.1021/bm201008b.
(20) Schrof, S.; Varga, P.; Galvis, L.; Raum, K.; Masic, A. 3D Raman Mapping of the Collagen Fibril Orientation in Human Osteonal Lamellae. *J. Struct. Biol.* **2014**, *187* (3), 266–275. https://doi.org/10.1016/j.jsb.2014.07.001.
(21) Bergholt, M. S.; St-Pierre, J. P.; Offeddu, G. S.; Parmar, P. A.; Albro, M. B.; Puetzer, J. L.; Oyen, M. L.; Stevens, M. M. Raman Spectroscopy Reveals New Insights into the Zonal Organization of Native and Tissue-Engineered Articular Cartilage. *ACS Cent. Sci.* **2016**, *2* (12), 885–895. https://doi.org/10.1021/acscentsci.6b00222.
(22) Lu, H.; Hoshiba, T.; Kawazoe, N.; Koda, I.; Song, M.; Chen, G. Cultured Cell-Derived Extracellular Matrix Scaffolds for Tissue Engineering. *Biomaterials* **2011**, *32* (36), 9658–9666. https://doi.org/10.1016/j.biomaterials.2011.08.091.
(23) Hurd, S. A.; Bhatti, N. M.; Walker, A. M.; Kasukonis, B. M.; Wolchok, J. C. Development of a Biological Scaffold Engineered Using the Extracellular Matrix Secreted by Skeletal Muscle Cells. *Biomaterials* **2015**, *49*, 9–17. https://doi.org/10.1016/j.biomaterials.2015.01.027.
(24) Pelletier, M. J. Quantitative Analysis Using Raman Spectrometry. *Appl. Spectrosc.* **2003**, *57*, 20A-42A.
(25) Shrirao, A. B.; Kung, F. H.; Yip, D.; Firestein, B. L.; Cho, C. H.; Townes-Anderson, E. A Versatile Method of Patterning Proteins and Cells. *J. Vis. Exp.* **2017**, No. 120, 1–8. https://doi.org/10.3791/55513.
(26) Bashey, R. I.; Martinez-Hernandez, A.; Jimenez, S. A. Isolation, Characterization, and Localization of Cardiac Collagen Type VI: Associations with Other Extracellular Matrix Components. *Circ. Res.* **1992**, *70* (5), 1006–1017. https://doi.org/10.1161/01.res.70.5.1006.
(27) Silva, A. C.; Pereira, C.; Fonseca, A. C. R. G.; Pinto-do-Ó, P.; Nascimento, D. S. Bearing My Heart: The Role of Extracellular Matrix on Cardiac Development, Homeostasis, and Injury Response. *Frontiers in Cell and Developmental Biology*. 2021, p 6211644. https://doi.org/10.3389/fcell.2020.621644.
(28) Csapo, R.; Gumpenberger, M.; Wessner, B. Skeletal Muscle Extracellular Matrix – What Do We Know About Its Composition, Regulation, and Physiological Roles? A Narrative Review. *Frontiers in Physiology*. 2020, p 253. https://doi.org/10.3389/fphys.2020.00253.
(29) Ferdman, A. G.; Yannas, I. V. Scattering of Light from Histologic Sections: A New Method for the Analysis of Connective Tissue. *J. Invest. Dermatol.* **1993**, *100* (5), 710–716. https://doi.org/10.1111/1523-1747.ep12472364.
(30) Tan, Y. Y.; Shen, A. G.; Zhang, J. W.; Wu, N.; Feng, L.; Wu, Q. F.; Ye, Y.; Hu, J. M. Design of Auto-Classifying System and Its Application in Roman Spectroscopy Diagnosis

of Gastric Carcinoma. *Int. Conf. Mach. Learn. Cybern.* **2003**, *3*, 1360–1363. https://doi.org/10.1109/ICMLC.2003.1259703.

(31) Cheng, W. T.; Liu, M. T.; Liu, H. N.; Lin, S. Y. Micro-Raman Spectroscopy Used to Identify and Grade Human Skin Pilomatrixoma. *Microsc. Res. Tech.* **2003**, *68* (2), 75–79. https://doi.org/10.1002/JEMT.20229.

(32) Columbia, B.; Columbia, B.; General, V.; Columbia, B. Near-Infared Raman Sspectroscopy for Optical Diagnosis of Lung Cancer. *Int. J. Cancer* **2003**, *107*, 1047–1052. https://doi.org/10.1002/ijc.11500.

(33) Stone, N.; Kendall, C.; Shepherd, N.; Crow, P.; Barr, H. Near-Infrared Raman Spectroscopy for the Classification of Epithelial Pre-Cancers and Cancers. *J. Raman Spec* **2002**, *33*, 564–573. https://doi.org/10.1002/jrs.882.

(34) Stone, N.; Kendall, C.; Smith, J.; Crow, P.; Barr, H. Raman Spectroscopy for Identification of Epithelial Cancers. *Faraday Discuss* **2004**, *126*, 141–157. https://doi.org/10.1039/b304992b.

(35) Notingher, I.; Green, C.; Dyer, C.; Perkins, E.; Hopkins, N.; Lindsay, C.; Larry, L.; Notingher, I.; Green, C.; Dyer, C.; Perkins, E.; Hopkins, N.; Lindsay, C.; Hench, L. L. Discrimination between Ricin and Sulphur Mustard Toxicity in Vitro Using Raman Spectroscopy. *J. R. Soc. Interface* **2004**, *1*, 79–90. https://doi.org/10.1098/rsif.2004.0008.

Supporting Information

Label-free quantification of alignment in engineered tissue scaffolds by polarized Raman spectroscopy

Hui Zhou[1+], Janny Piñeiro Llanes[2], Maedeh Lotfi[1], Malisa Sarntinoranont[1], Chelsey S. Simmons[1] and Ghatu Subhash[1*]

[1]Mechanical and Aerospace Engineering, University of Florida, Gainesville, Florida 32611, United States
[2]J. Crayton Pruitt Family Department of Biomedical Engineering, University of Florida, Gainesville, Florida 32611, United States
+Current Address: Collage of Polymer Science and Engineering, State Key Laboratory of Polymer Materials and Engineering, Sichuan University, Chengdu, 610065

Corresponding Author
* Email: subhash@ufl.edu

This PDF file includes:
1. Supplementary Appendix 1Methods
2. Supplementary Table S1-S3 and supplementary Figure S1-S4
3. Supplementary Appendix 2. MATLAB routine for Preprocessing and PCA analysis
4. References

Supplementary Appendix S1 Methods

A. Preparation of cardiac fibroblasts

The differentiation of hPSCs to cardiac fibroblasts (CFs) followed by a previously published protocol.[1] hPSCs were generated from foreskin-derived fibroblasts of a healthy male adult by using the cytoTune Sendai virus reprogramming kit as previously described.[2] hPSCs were approved for use under UF IRB201400246 and were seeded on Matrigel (Corning, 354230) coated 6-well plates in mTeSRTM Plus medium (StemCell Technologies, 05825)and cultured at 37˚C, 5% CO2. The medium was changed every day until the cells reached 100% confluency and the differentiation started (day 0). At day 0, cells were cultured in the medium replaced by 2.5 ml RPMI (Gibco A10491-01)+B27without insulin (Gibco A1895601) and supplemented with 12 μM CHIR99021(Tocris 4423l) for 24 h (day 1). After day 1, the cells were treated in the

medium of 2.5 ml RPMI+B27 without insulin for 36 h (day 2.5). At day 2.5, the cells were cultured in 2.5 ml of the cardiac fibroblast basal differentiation medium (CFBM; Cell Applications, 315-500) supplemented with 75 ng/ml bFGF (Gibco 13256029). Until day 20, the cells were fed with CFBM + 75ng/ml bFGF every day with medium changed every other day. All hPSC-CFs were cryopreserved in 90% FBS and 10% DMSO.

B. Additional notes for PBS data acquisition and analysis

B1. PRS calibration

Polarized Raman spectroscopy was performed on the sample in a Invia™ Reflex Raman microscope coupled with polarizer (Renishaw plc., Gloucester, UK) with a 532 nm continuous wave solid-state laser (Renishaw A-9836-5053) and 20X water dipping lens (N.A.=0.5). The spatial resolution is around 1 μm and spectral resolution is around 6.8 cm^{-1} for this spectrometer. To keep consistence of each PRS measurement, an automated program for aligning optic elements in the light path should be performed. Otherwise, a deviation of any element(s) would influence the efficiency of Raman signal collection. Since our PRS method relies on variations of intensities in tissue samples, the results for analysis may become unreliable each time when alignment correction is not finished. This program is under “Auto Align” tab in WIRE software (Renishaw company), which you can run the Auto Align procedures by doing “Auto Align Si reference” followed by “Auto Laser Align”, “Auto CCD Align” and “Auto Align Slit”. For all, follow the on-screen instructions, and accept the final results. The linearity of Raman spectrometer should also be checked due to its impact on the Raman intensity. It can be performed by measuring with the internal neon calibration source and, after correcting the off-axis and chromatic aberration, the calibration shows precision and accuracy of Raman

wavenumbers should be less than 1 cm^{-1}. Another calibration is for calibrating the position of Raman band, namely "wavenumber" on the x axis of a Raman spectrum. If the position calibration is not checked, a Raman peak coming from the same chemical bond may shift in the x axis (wavenumber). Hence the intensity of each Raman band in a given wavenumber may change, which would affect PCA analysis (highly depended on the intensity values for each wavenumber). To do the position calibration, firstly, the internal Si calibration program is run in WIRE software by selecting "Internal Si Reference Measurement" to calibrate. If the peak of Si in the Raman spectrum is not in the 520-521 cm^{-1} range, run the calibration again until it follows within the range. Alternatively, you can calibrate the Raman shift by putting the offset value (positive if the Si peak is greater than 521 cm^{-1}). Secondly, an external source is used as reference sample, which is crystal silicon (100). Run Raman measurement and obtain its Raman spectrum and check if the position of peak is around 520.5 ± 0.5 cm^{-1} (A standard Si sample should show a Raman peak at 520.5 cm^{-1}). Run the calibration again until it follows within the range. For correction of dark current, since the spectra were acquired using a charged-coupled device (CCD) camera EMCCD (Newton DU970P; Oxford Instruments plc, Concord, MA, USA) and it was thermoelectrically cooled down to -100 °C, the dark current is negligible. Moreover, polarized Raman measurement needs the calibration of the light polarization in the system, Prior to measurements on ETC samples, the Renishaw InVia was checked for instrumental polarization effects by measuring depolarization ratios of CCl_4. The definition of the depolarization ratio is the intensity ratio between the perpendicular component and the parallel component of Raman scattered light.[3] Followed by the physical law, the depolarization ratio of the totally symmetric stretch should be close to zero while the ratios of remaining non-totally symmetric bands should close to 0.75.[4] Within experimental errors, these ratios should be

observed to be similar to those reported in literature, showing no significant polarization dependence of the Raman spectrometer. If it is not calibrated, the intensity collected at different polarized angles may not be reliable across different measurements. This may affect the PCA analysis result and further quantification of Amplitude Alignment Metric (AAM). Lastly, Raman spectra of the optical background were averaged out and was used to be subtracted from spectra of tissue samples.

B2. PRS characterization

The parameters about PRS characterization were set as follows:

Table S1. The parameters set for PRS measurement

Parameters	Values/Settings
Laser wavelength	532 nm
Laser power	50 mW
Laser exposure time	10s
Accumulation number	12
Cosmic ray removal	Yes
Collected spectral range	centered at 1450 cm^{-1}

B3. Sine fitting and amplitude caculation

$$\text{PC1 Score} = y = y_0 + A \sin\left(\frac{\pi(x - x_c)}{w}\right) \quad \text{(S1)}$$

where y is the PC1 Score, y_0 is y-offset for the sine fit, A is amplitude of the sine fit, w is period, x_c is the phase shift and x is the experimental polarization angle (in degrees) between the sample alignment axis and polarized direction. x_c is fixed prior to sine fitting by calculating where the maximal difference of PC1 Score for a pair of polarized angles (separated by 90º) occurs. For example, if the largest difference between PC1 Score is observed between 0˚ (positive PC1 Score) and 90˚ (negative PC1 Score), then x_c = -45˚.All the fitting parameters were set as below:

Table S2. The parameters set for sine fitting

Parameters	Settings	Descriptions
w	90˚	90˚ follows natural periodicity of protein fiber distributions
x_c	Fixed	x_c depends on where the maximal difference of PC1 Score occurs
y_0	Unfixed	Unfixed y_0 allows adjusting bias in data and avoids overfitting
A	-	*So-called "*Amplitude Alignment Metric", indicating alignment

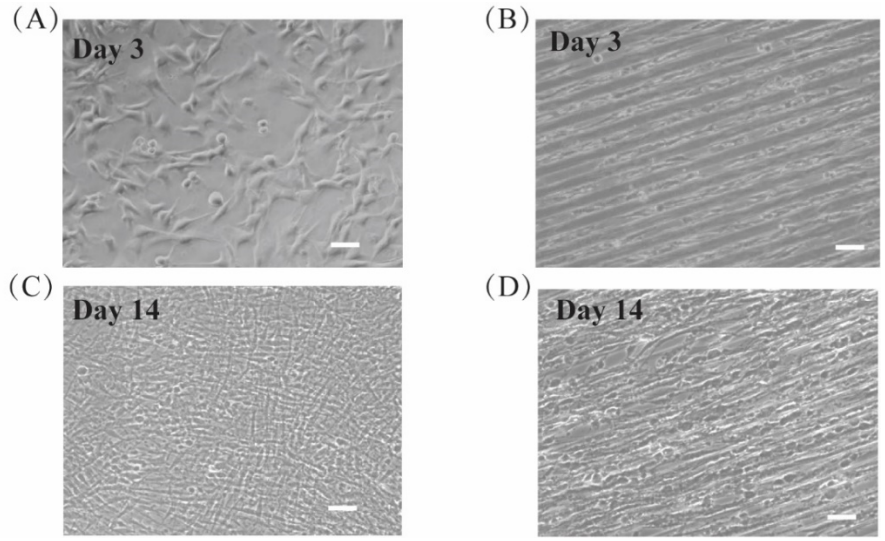

Figure S1. The phase contrast images of (A) aETSs and iETS cultured for day 3 and (C)aETS and iETS cultured day 14.

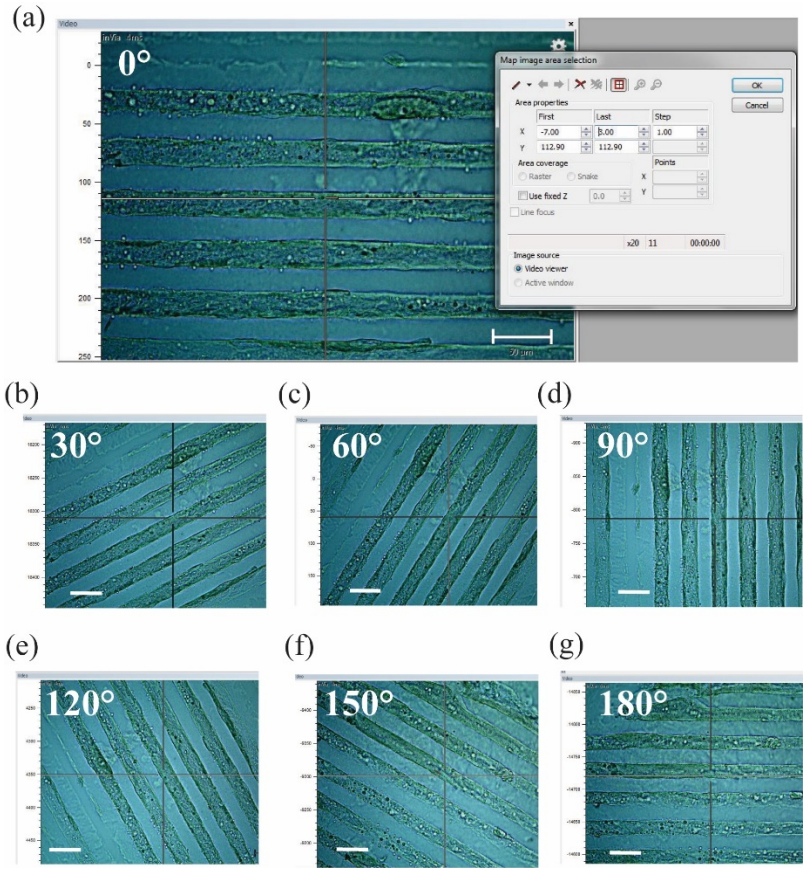

Figure S2. The bright field image of ETS samples before PRS measurement. A10 μm region of interest (ROI) was scanned at a step size of 1 μm for PRS measurement (a) at 0˚ polarized angle. And the same ROI was characterized for PRS measurement at (b)30˚, (c)60˚, (d)90˚, (e)120˚, (f)150˚ and (g)180˚, respectively. Scale bar = 50 μm.

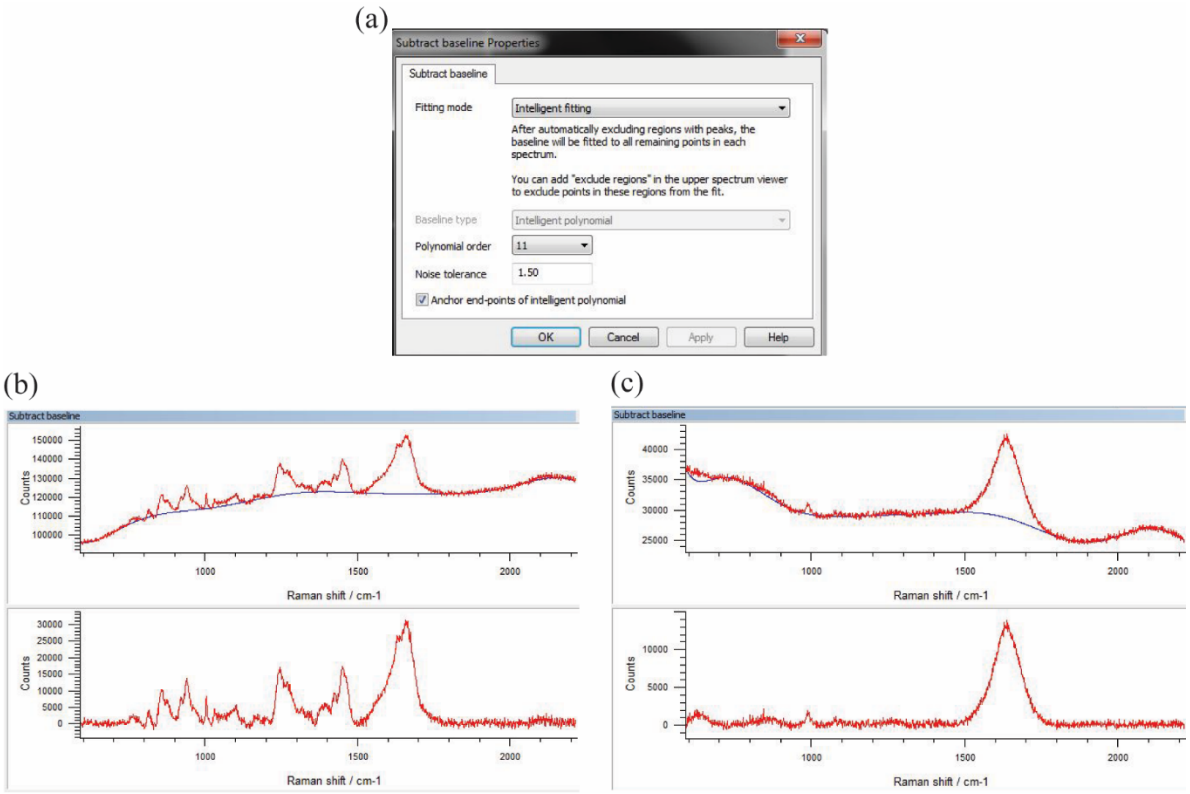

Figure S3. The polynomial fitting for subtracting fluorescence background from Raman spectra. (a) Subtraction parameters were set for all the spectra with 11th order polynomial fitting for background and noise filter=1.5 and this 11th order polynomial subtraction was performed for (b) spectrum of ETS an (c) spectrum of PBS, respectively (upper panel for fitting fluorescence background; lower panel showing spectra after subtraction).

Table S3. The raw values of R-square for sine fittings for aETS and iETS

aETS	iETS
0.24	0.27
0.39	0.27
0.27	0.05
0.46	0.05
0.37	0.11
0.10	0.46
0.43	0
0.76	0.04
0.57	0.05
0.40	0.08
0.39	0.07
0.22	0.24

0.36	0.21
0.51	0
0.72	0.30
0.49	0.06
0.59	0.68
0.47	0.15
0.54	0.11
0.50	0
0.74	0

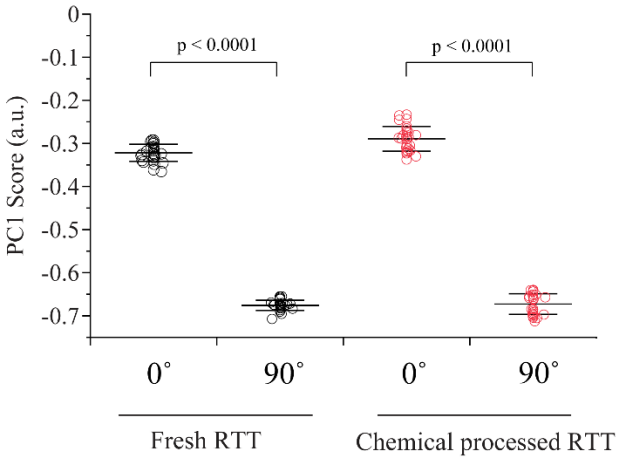

Figure S4. Chemical fixation has minimal effect on ability of PC1 Score to characterize (an)isotropy for rat tail tendon (RTT). The figure shows PC1 Score of fresh RTT vs fixed RTT (n=30 per group) at 0˚ and 90˚ polarized angles. Processed RTT refers to the RTT that was processed with 70% ethanol, 70% isopropanol and acetone sequentially.

Appendix S2. MATLAB routine for Preprocessing and PCA analysis

```
%Preprocess part(i) Raman spectra and part (ii)PCA analysis
%Read Raman text files respectively from 0° to 180°(7 angles in total)
%Each angle consists of ROI1(11 Locs)&ROI2(11 Locs)
for ii=0:30:180
filename1 = sprintf('Muscle%d_1.txt',ii);
filename2 = sprintf('Muscle%d_2.txt',ii);
filename3 = sprintf('Muscle%d_pbs.txt',ii);
M1 = dlmread(filename1); %read raw data of ROI1 into M1
M2 = dlmread(filename2); %read raw data of ROI2 into M2
PBS = dlmread(filename3); %read raw PBS into PBS
X= M1(751:1153,3); %read 1400 to 1800 cm-1 wavenumber
%adjust location order in each angle:
%"0" means keeping original order while "-12" means keep opposite order
adj1=[0 0 0 0 -12 -12 -12]; %adj1:adjust order of ROI1 from 0° to 180°
adj2=[0 0 0 0 -12 -12 -12]; %adj2:adjust order of ROI2 from 0° to 180°
% read spectra in 1400-1800cm-1 range for ROI1, ROI2&PBS
for i =1:1:11
    i0 = abs(i+adj1(ii/30+1)); %"adj1(ii/30+1)" adjust order for each angle
    Y(:,i) = M1((750+1600*(i0-1)):(1152+1600*(i0-1)),4); %read ROI1
end
for j=1:1:11
    j0= abs(j+adj2(ii/30+1)); %"adj2(ii/30+1)" adjust order for each angle
    Y(:,11+j)= M2((750+1600*(j0-1)):(1152+1600*(j0-1)),4); %read ROI2
end
```

```
for k = 1:1:5
    P(:,k) = PBS((750+1600*(k-1)):(1152+1600*(k-1)),3); %read PBS
end
P_ave = mean(P,2); %average of PBS measured 5 times
YS=Y-P_ave; %subtraction of PBS background

%smoothing by Savitzky-Golay filtering with 3th order, window size=11
order = 3;
framelen = 11;
sgfYS = sgolayfilt(YS,order,framelen);
plot(X,YS,':') %plot raw spectra
hold on
plot(X,sgfYS,'.-') %plot smoothed spectra
legend('signal','sgolay')
title('Unnormalized')
drawnow
%SNV normalization for 2ROI*11 locations= 22 spectra
hFig=figure;
Mean=mean(sgfYS);
Std=std(sgfYS);
SNV_Y= (sgfYS-Mean)./Std;
plot(X,SNV_Y,'-');
legend show
SNVY(1:403,1+22*(ii/30):22*(ii/30+1))=SNV_Y;

title('SNV Normalized')
end
xlswrite('SNVY.xlsx',SNVY) %save preprocessed 22 spectra in excel
close(hFig)
% plot preprocessed Raman spectra of 22 locations for each angle
for t= 1:7
    figure(8+t)
    plot(X,SNVY(:,1+22*(t-1):22*t))
    t1=30*(t-1);
    title(sprintf('polarized angle%d',t1))
    legend show
end
```

```
% PCA analysis
% Get PC1 Score by subtracting mu from SNVY data and multiplying by coeff
coeff = xlsread('Loading coeff.xlsx');
mu = mean(SNVY,2);
SNVYS = SNVY-mu;
coeffPC = coeff.';
PC1_Score = coeffPC*SNVYS;
% standarized PC1 Score
u = mean(PC1_Score);
SD = std(PC1_Score);
PC1_std = (PC1_Score-u)./SD;
PC1 = zeros(7,22);
for p = 1:1:22
    PC1(:,p) = PC1_std(1,22*((0:6))+p);
end
angle = [0;30;60;90;120;150;180];
plot(angle, PC1, '+b'); %plot PC1 Score for 7 angles(each: 22locations)
axis([-20 220    -3.5  3.5]);
xlabel('Polarized Angle (\circ)');
ylabel('PC1 Score (a.u.)');
ave_PC1 =mean(PC1,2);
fin_PC1= [PC1 ave_PC1];
%Save PC1 in excel, LAST COLUMN!! is averaged PC1 Score per angle
```

```
%%
%to find optimized shift angle Xc to fit sine fit
diff_PC1=[1/2*(abs(ave_PC1(1)-ave_PC1(4))+abs(ave_PC1(4)-ave_PC1(7)));
abs(ave_PC1(2)-ave_PC1(5));
abs(ave_PC1(3)-ave_PC1(6))];
[Max,Index] = max(diff_PC1);
if (Index == 1)&&(ave_PC1(1)>ave_PC1(4))&&(abs(ave_PC1(1)-ave_PC1(4))>abs(ave_PC1(4)-ave_PC1(7)))
    disp('phase angle should be set: xc=-45 degree')
elseif (Index == 1)&&(ave_PC1(1)<ave_PC1(4))&&(abs(ave_PC1(1)-ave_PC1(4))>abs(ave_PC1(4)-ave_PC1(7)))
    disp('phase angle should be set: xc=45 degree')
elseif (Index == 1)&&(ave_PC1(4)<ave_PC1(7))&&(abs(ave_PC1(1)-ave_PC1(4))<abs(ave_PC1(4)-ave_PC1(7)))
    disp('phase angle should be set: xc=-45 degree')
elseif (Index == 1)&&(ave_PC1(4)>ave_PC1(7))&&(abs(ave_PC1(1)-ave_PC1(4))<abs(ave_PC1(4)-ave_PC1(7)))
     disp('phase angle should be set: xc=45 degree')
elseif (Index == 2)&&(ave_PC1(2)>ave_PC1(5))
    disp('phase angle should be set: xc=-15 degree')
elseif (Index == 2)&&(ave_PC1(2)<ave_PC1(5))
    disp('phase angle should be set: xc=75 degree')
elseif (Index == 3)&&(ave_PC1(3)>ave_PC1(6))
    disp('phase angle should be set: xc=15 degree')
else (Index == 3)&&(ave_PC1(3)<ave_PC1(6))
     disp('phase angle should be set: xc=-75 degree')
end
```

References

(1) Zhang, J.; Tao, R.; Campbell, K. F.; Carvalho, J. L.; Ruiz, E. C.; Kim, G. C.; Schmuck, E. G.; Raval, A. N.; da Rocha, A. M.; Herron, T. J.; Jalife, J.; Thomson, J. A.; Kamp, T. J. Functional Cardiac Fibroblasts Derived from Human Pluripotent Stem Cells via Second Heart Field Progenitors. *Nat. Commun.* **2019**, *10* (1). https://doi.org/10.1038/s41467-019-09831-5.

(2) Watanabe, N.; Kitada, K.; Santostefano, K. E.; Yokoyama, A.; Waldrop, S. M.; Heldermon, C. D.; Tachibana, D.; Koyama, M.; Meacham, A. M.; Pacak, C. A.; Terada, N. Generation of Induced Pluripotent Stem Cells from a Female Patient with a Xq27.3-Q28 Deletion to Establish Disease Models and Identify Therapies. *Cell. Reprogram.* **2020**, *22* (4), 179–188. https://doi.org/10.1089/cell.2020.0012.

(3) Iwata, K.; Weaver, W. L.; Gustafson, T. L. Time Dependence of the Depolarization Ratio in Picosecond Time-Resolved Raman Spectroscopy. Effect of Reorientation. *Chem. Phys. Lett.* **1993**, *210* (1–3), 50–54. https://doi.org/10.1016/0009-2614(93)89098-3.

(4) Chakraborty, T.; Rai, S. N. Depolarization Ratio and Correlation between the Relative Intensity Data and the Abundance Ratio of Various Isotopes of Liquid Carbon Tetrachloride at Room Temperature. *Spectrochim. Acta Part A Mol. Biomol. Spectrosc.* **2005**, *62* (1–3), 438–445. https://doi.org/10.1016/J.SAA.2005.01.012.